Orbital degeneracy as a source of frustration in LiNiO$_2$

F. Vernay,[1] K. Penc,[2] P. Fazekas,[2] and F. Mila[1]

[1]*Institute of Theoretical Physics, Ecole Polytechnique Fédérale de Lausanne, CH-1015 Lausanne, Switzerland*
[2]*Research Institute for Solid State Physics and Optics, P.O. Box 49, H-1525 Budapest, Hungary*

Motivated by the absence of cooperative Jahn-Teller effect and of magnetic ordering in LiNiO$_2$, a layered oxide with triangular planes, we study a general spin-orbital model on the triangular lattice. A mean-field approach reveals the presence of several singlet phases between the SU(4) symmetric point and a ferromagnetic phase, a conclusion supported by exact diagonalizations of finite clusters. We argue that one of the phases, characterized by a large number of low-lying singlets associated to dimer coverings of the triangular lattice, could explain the properties of LiNiO$_2$, while a ferro-orbital phase that lies nearby in parameter space leads to a new prediction for the magnetic properties of NaNiO$_2$.

I. INTRODUCTION

The Mott insulators LiNiO$_2$ and NaNiO$_2$ are isostructural and isoelectronic, but they have completely different phase diagrams. The complicated nature of these systems arises from an interplay of the dynamical frustration of spin–orbital models with the geometrical frustration of the triangular lattice, which is the essential structural unit. We will show that by a modest change of parameters, a great variety of phases can be derived.

The crystal structure can be envisaged as a sequence of slabs of edge-sharing octahedra of oxygen O^{2-} ions. Metal ions sit at the centers of octahedra. There are two kinds of slabs: in A slabs, at every center of octahedra there is a Ni^{3+}, whereas in the B slabs, one finds either Li$^+$ or Na$^+$ ions. A and B slabs alternate (see Fig. 1). The Ni ions form well-separated triangular planes.

It is useful to start with the idealized geometry of a cubic system. Neglecting the inequivalence of Ni and Li sites, and assuming perfect oxygen octahedra, the octahedral centers would form a simple cubic lattice. The slabs of the original structure would be perpendicular to the 111 direction. Within a slab the Ni-O-Ni bond angles would be 90°, resulting in important consequences for the effective exchange.[1]

There are two sources of deviation from cubic symmetry: (a) Ni and Li/Na sites are inequivalent, which leaves us with one (instead of four) C$_3$ axis. Even if the octahedra were undistorted, Ni ions would see a wider environment with trigonal symmetry only. (b) actually, oxygen octahedra are distorted,[2,3] and the Ni$-$O$-$Ni bond angle is $\approx 96.4°$ in the case of Na, and $\approx 94°$ in case of the Li compound.

If there is a Jahn–Teller phase transition (as in NaNiO$_2$), it lowers the crystal symmetry further and makes the orbital ground state unique. An alternative would be to ascribe orbital polarization to an electronic phase transition due to orbital exchange and to regard the lattice distortion as an induced secondary effect. In what follows, we assume trigonal point group symmetry, which is valid for NaNiO$_2$ at high temperatures and for LiNiO$_2$ at all temperatures. Breaking the local trigonal symmetry, whenever it happens, is ascribed to orbital ordering. We consider electronic degrees of freedom only, but we assume that the lattice would follow the changing orbital occupation.

The Ni^{3+} ions are in the $S=1/2$ low-spin state. In terms of the dominant cubic component of the crystal field $3d^7 = t_{2g}^6 e_g^1$. Since the actual point group symmetry is trigonal, t_{2g} gets split into two levels ($t_{2g} \rightarrow A_2 + E$, where standard notations for the irreducible representations (irreps) of the point group $\mathcal{D}_{3d}$ were introduced), but this does not affect the fact that six electrons are taken up by closed subshells, and only the seventh electron is in an open subshell. The trigonal crystal field component changes the detailed nature of the d-states, but still allows for twofold orbital degeneracy: $e_g^{\text{cubic}} \rightarrow E$. In what follows, E is understood to denote the two-dimensional (2D) irrep of the trigonal point group.[4]

The ground state of an isolated Ni^{3+} ion is fourfold degenerate: it has twofold orbital and twofold spin degeneracy. A standard scenario would be that the non-Kramers degeneracy is resolved by a (cooperative) Jahn–Teller effect, while the Kramers degeneracy is lifted by magnetic ordering. Let us note that, as far as the E-electrons are concerned, the cooperative Jahn–Teller effect is synonymous with orbital ordering, thus it can be explained with a purely electronic model, without the consideration of electron–lattice coupling.
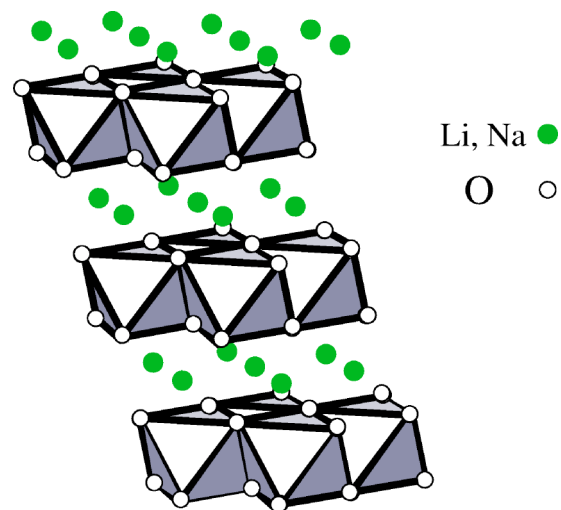
FIG. 1. ANiO$_2$ structure. Ni ions are located in the middle of the O octahedra.

Li, Na ●

O ○

The standard scenario seems to be (at least nearly) realized for NaNiO$_2$, which has a first-order cooperative Jahn-Teller transition lowering the local symmetry from trigonal to monoclinic at $T_{JT}^{Na} \sim 480$ K.[2] The remaining Kramers degeneracy is lifted by a magnetic transition at $T_N^{Na} \approx 20$ K, which was characterized as the antiferromagnetic ordering of ferromagnetic planes.[5] In contrast, LiNiO$_2$ does not undergo a Jahn–Teller distortion,[6] and though the measured susceptibility shows a number of anomalies, it does not seem to develop magnetic long-range order.[3,7,8] It is puzzling that the two isostructural and isoelectronic compounds show such different behavior. Naturally, it is always possible that some of the observed behavior is not intrinsic. Impurities and structural defects are likely to prevent orbital ordering. Indeed, it was suggested that only NaNiO$_2$ allows the growth of sufficiently good-quality samples, and the observation of ordering transitions, while the overall behavior of LiNiO$_2$ is like that of the high-temperature phase of NaNiO$_2$.[2]

II. SPIN–ORBITAL MODEL BASED ON THE TRIGONAL DOUBLET

The aim of the present paper is to show that the contrasting features of NaNiO$_2$ and LiNiO$_2$ appear naturally as nearly equivalent possibilities for the intrinsic behavior of spin-orbital models of the trigonal E doublet.

A similar four-state model, namely the $S=1/2$ cubic e_g doublet on the cubic lattice, has been studied in great detail in the context of manganite physics.[9] The magnetic behavior is complicated because orbital and spin–orbital interactions tend to frustrate the usual spin–spin interactions. Though, in contrast to spin-only models, spin–orbital models do not need the fine-tuning of the lattice structure to get frustration effects, we find that the geometrical frustration of the triangular planes of the LiNiO$_2$ structure brings essential new features. For this reason, we consider only an isolated triangular plane and discuss $T=0$ behavior only. We assume that our essential conclusions would carry over to the $T>0$ behavior of coupled planes.

The idea that the geometrical frustration of the triangular lattice tends to oppose ordering has been discussed for spin[10,11] and orbital[12] degrees of freedom separately. In a pioneering work, Hirakawa, Kadowaki, and Ubukoshi[13] started a systematic investigation of triangular lattice antiferromagnets with the explicit aim of finding non-Néel-type behavior. This work initiated the intensive reinvestigation of LiNiO$_2$. On the theoretical side, Arimori and Miyashita [14] studied a classical model and found that novel-order parameters combining spin and orbital character are important. In a quantum-mechanical calculation, chosing a special set of parameters to make the four-state spin-orbital model SU(4) symmetrical, it was found that the ground state of the nearest-neighbor model on the triangular lattice is an SU(4)-resonating quantum liquid.[15]

Here we consider the full range of E models, restricting the parameters only by the requirements dictated by symmetry. The pair interaction is generically of SU(2)$\otimes C_{2h}$ symmetry; higher symmetries [SU(2)$\otimes$SU(2) or SU(4)] follow from specific choices of the parameters. We explore many

lower-symmetry states in addition to the fully symmetrical SU(4) phase. Accepting that the observed behavior of both LiNiO$_2$ and NaNiO$_2$ is intrinsic, any theory for why LiNiO$_2$ does not order should also allow for the alternative scenario of orbital and spin ordering, as observed in NaNiO$_2$. In terms of our trigonal E model, we show that the combination of geometrical frustration with the dynamical frustration inherent in spin-orbital models gives rise to a rich variety of competing states stretching from the SU(4) resonating singlet-state to spin-ferromagnetic phases with various orbital order. We will find it natural that contrasting behavior resembling that of either LiNiO$_2$ or NaNiO$_2$ can arise in nearby regions of parameter space.

A. Basis functions

Our model is meant to describe the Mott-localized E electrons of Ni ions. The local degrees of freedom are those of an E^1 shell. Intersite interactions arise from the virtual charge fluctuations $E^1E^1 \rightarrow E^2E^0$. The study of such spin-orbital exchange models was initiated by Kugel and Khomskii,[16] and by Castellani, Natoli, and Ranninger.[17]

The point group of a Ni site is $\mathcal{D}_{3d}=\mathcal{D}_3 \otimes \{\mathcal{E}, \mathcal{I}\}$, where $\mathcal{E}$ is the identity element, and $\mathcal{I}$ is the inversion. (see Fig. 2) The subgroup of proper rotations $\mathcal{D}_3$ contains the trigonal axis $\mathcal{C}_3$ and three orthogonal $\mathcal{C}_2$ axes. It is convenient to denote axes in terms of the original octahedral system $\{X, Y, Z\}$, so the $\mathcal{C}_3$ axis is (111). For later reference, we recall that $\mathcal{D}_{3d}$ has three irreps: the identity rep A_1, the one-dim irrep A_2, and the two-dim irrep E.

First, we represent $\mathcal{D}_3$ on the basis of the E subspace spanned by $c_a^\dagger|0\rangle=|a\rangle \propto (3Z^2-R^2)$, and $=c_b^\dagger|0\rangle=|b\rangle \propto (X^2-Y^2)$ (as yet, we omit the spin index). Alternatively, we may represent on the 2D operator subspaces $\{c_a^\dagger, c_b^\dagger\}$ (or $\{c_a, c_b\}$). The effect of a π-rotation about the $1\bar{1}0$ axis (one of the C_2 axes) is

$$c_{a'}^\dagger = c_a^\dagger, \quad c_{b'}^\dagger = -c_b^\dagger. \tag{1}$$

Skipping the effect of the other two $\mathcal{C}_2$ rotations, we show how a $2\pi/3$ rotation about the trigonal axis is represented in the E subspace

$$c_{a'}^\dagger = -\frac{1}{2}c_a^\dagger + \frac{\sqrt{3}}{2}c_b^\dagger$$

$$c_{b'}^\dagger = -\frac{\sqrt{3}}{2}c_a^\dagger - \frac{1}{2}c_b^\dagger. \tag{2}$$

B. Microscopic model

On-site d-electron orbital states are classified according to the point group $\mathcal{D}_{3d}$,[18] while two-site states according to the smaller point group C_{2h} of a pair. The nearest neighbors of a Ni site are at the centers of octahedra, which share an edge with the first site. The C_2 axis perpendicular to this edge is a symmetry element of the pair; so is the mirror plane σ_h perpendicular to the C_2 axis in question.[19] C_2 and σ_h are the
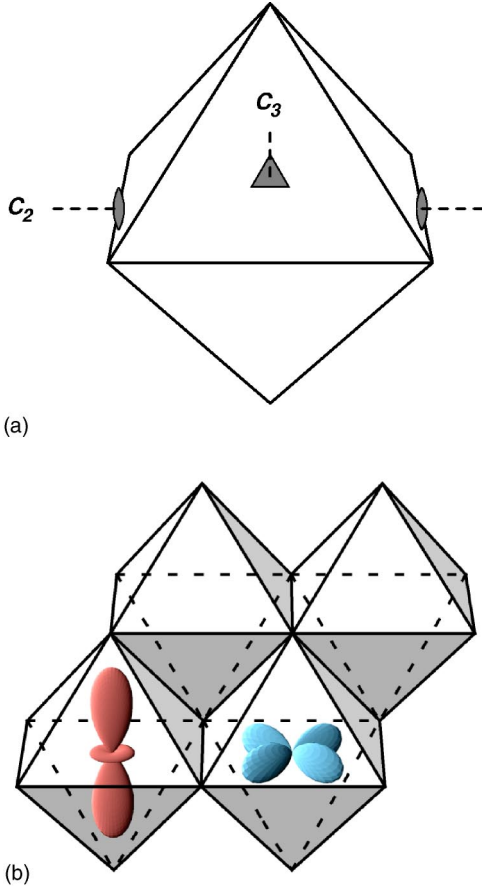
FIG. 2. (a) The $\mathcal{C}_3$ axis and one of the $\mathcal{C}_2$ axes of the point group of the Ni site in the $ANiO_2$ structure (the other two $\mathcal{C}_2$ axes are obtained by applying $\mathcal{C}_3$). (b) Orbital states of the seventh d-electron of Ni^{3+} on the background of the network of oxygen octahedra.

generators of the four-element symmetry group $\mathcal{C}_{2h}$ of the pair.[20]

The standard components of the electronic Hamiltonian are those of a two-band extended Hubbard model: intersite hopping H_{hop} and on-site Coulomb matrix elements $\mathcal{H}_{\text{Coul}}$. First, we discuss $\mathcal{H}_{\text{hop}}$. The local E basis can always be chosen so that under the $\mathcal{C}_2$ rotation of the pair, one of the basis states is even, and the other is odd. In fact, we have seen this in (1). This immediately implies that the hopping elements between two sites are only between the functions with equal parity, and we have two hopping parameters only: t for the a orbitals, and t' for the b orbitals

$$\mathcal{H}_{\text{hop}} = -t \sum_\sigma c_{i,a,\sigma}^\dagger c_{j,a,\sigma} - t' \sum_\sigma c_{i,b,\sigma}^\dagger c_{j,b,\sigma} + \text{H.c.} \quad (3)$$

where σ is the spin index. In the other directions the hopping amplitudes can be obtained by a suitable rotation of the basis functions and the hopping matrix. Let us note that for pairs with a different orientation, inter-orbital hopping terms will be generated.

a and b need not mean strictly Ni d-states, but rather more extended one-electron states of the same symmetry. Since one of the main pathways of electron propagation would be through the oxygen network, we should think of the orbitals as hybridized Ni-centered Wannier orbitals, but with hopping amplitudes that follow not only from Ni–O–Ni hybridization, but by considering all finite-amplitude processes that are symmetry-allowed, and which in the end-effect, may be indexed in the same way as the simple nearest-neighbor Ni–Ni hopping.

It was noted by Mostovoy and Khomskii[1] that the assumption of an exactly 90° Ni–O–Ni bond angle results in a peculiar form of the spin-orbital effective Hamiltonian. In particular, spin-spin coupling is exclusively ferromagnetic, and orbital exchange predominates. One of the ways to look at the situation is that, with an ideal octahedron of oxygen atoms, one-electron terms would not allow the propagation of an electron from a Ni site to another Ni site via an intervening oxygen atom. However, other off-diagonal elements, like the spin flip part of the p-shell Hund coupling, still allow electron propagation, and a corresponding term in spin-orbital exchange.[1] This model may be used to describe $NaNiO_2$, but it is certainly not applicable to $LiNiO_2$. Since we aim at deriving both kinds of behavior from formally the same Hamiltonian, we have to pay particular attention to the sources of deviation from the Mostovoy-Khomskii scheme.

Daré, Hayn, and Richard[21] pointed out that the trigonal splitting of the oxygen p orbitals, and the deviation of the Ni–O–Ni bond angle from 90°, facilitate the appearance of antiferromagnetic Ni–Ni interactions. However, they did not systematically explore the phase diagram, and neglected several effects that we think are important: the direct overlap of the Ni wave functions at neighboring sites, and the intra-atomic exchange and double hopping terms of the d-d interaction at Ni sites.[22] Our aim is a systematic investigation of the phase diagram in the entire parameter range.

The form of the on-site pair interaction term $\mathcal{H}_{\text{Coul}}$ is restricted by the symmetry classification of the two-electron states: $\mathcal{D}_{3d}$ for the orbital component of the wave function, and $SU(2)$ for the spin part, which readily gives three singlets and a triplet. Orbital quantum numbers follow from $E \otimes E = A_1 + A_2 + E$. The antisymmetrical A_2 can be taken with symmetrical spin states, yielding the triplet.

$$|F_1\rangle = c_{a,\uparrow}^\dagger c_{b,\uparrow}^\dagger |0\rangle$$

$$|F_2\rangle = \frac{1}{\sqrt{2}} (c_{a,\uparrow}^\dagger c_{b,\downarrow}^\dagger + c_{a,\downarrow}^\dagger c_{b,\uparrow}^\dagger) |0\rangle$$

$$|F_3\rangle = c_{a,\downarrow}^\dagger c_{b,\downarrow}^\dagger |0\rangle. \quad (4)$$

A_1 and E are symmetrical, thus there must be two singlet levels: the nondegenerate A_1, and the twofold degenerate E. The E-basis functions are

$$|F_4\rangle = \frac{1}{\sqrt{2}} (c_{a,\uparrow}^\dagger c_{b,\downarrow}^\dagger - c_{a,\downarrow}^\dagger c_{b,\uparrow}^\dagger) |0\rangle$$

$$|F_5\rangle = \frac{1}{\sqrt{2}} (c_{a,\uparrow}^\dagger c_{a,\downarrow}^\dagger - c_{b,\uparrow}^\dagger c_{b,\downarrow}^\dagger) |0\rangle \quad (5)$$

and the A_1-basis function is

$$|F_6\rangle = \frac{1}{\sqrt{2}}(c_{a,\uparrow}^\dagger c_{a,\downarrow}^\dagger + c_{b,\uparrow}^\dagger c_{b,\downarrow}^\dagger)|0\rangle. \tag{6}$$

Their transformation scheme under $\mathcal{C}_3$

$$|F_4'\rangle = -\frac{1}{2}|F_4\rangle + \frac{\sqrt{3}}{2}|F_5\rangle$$

$$|F_5'\rangle = -\frac{\sqrt{3}}{2}|F_4\rangle - \frac{1}{2}|F_5\rangle$$

follows from (2). The most general on-site two-body Hamiltonian describing the $E \otimes E$ set of levels is

$$\mathcal{H}_{\text{Coul}} = \frac{\widetilde{U}}{2}n^2 - J_H\left(\mathbf{S}_a\mathbf{S}_b + \frac{3}{4}n_a n_b\right) + J_p(c_{a,\uparrow}^\dagger c_{a,\downarrow}^\dagger + c_{b,\uparrow}^\dagger c_{b,\downarrow}^\dagger)$$
$$\times(c_{a,\downarrow}c_{a,\uparrow} + c_{b,\downarrow}c_{b,\uparrow}) \tag{7}$$

where the $\widetilde{U}$ is the familiar on-site repulsion of the Hubbard model, J_H is the Hund's coupling and J_p is the pair hopping amplitude. The spectrum of $\mathcal{H}_{\text{Coul}}$ consists of a triplet level at $\widetilde{U}-J_H$ ($|F_1\rangle$, $|F_2\rangle$, and $|F_3\rangle$), a twofold degenerate singlet at $\widetilde{U}$ ($|F_4\rangle$ and $|F_5\rangle$), and a nondegenerate singlet at $\widetilde{U}+2J_p$ ($|F_6\rangle$).

Since each of the single-site terms is invariant under rotations in the orbital space, $\mathcal{H}_{\text{Coul}}$ written in (7) is quite general, and its two independent parameters $J_H/\widetilde{U}$ and $J_p/\widetilde{U}$ could be chosen arbitrarily. We may think of these as effective interaction parameters, which encompass all allowed processes affecting the E level under consideration. According to the usual evaluation of the simple Coulomb interaction we get $J_p=J_H/2$. This physically motivated assumption was used by Castellani, Natoli, and Ranninger in their pioneering work [17] on V_2O_3. See Ref. 9 for further discussions of this point.

C. The effective Hamiltonian from symmetry considerations

The 4D Hilbert space of E^1 states supports 15 local-order parameters.[23] Their standard choice is S^x, S^y, S^z for the spins, T^x, T^y, T^z for the orbitals, and further nine operators S^xT^x, $S^xT^y,\dots$ of mixed spin-orbital character.[24] Here we introduced the $T=1/2$ pseudospin operators

$$T_i^x = \frac{1}{2}\sum_\sigma (c_{i,a,\sigma}^\dagger c_{i,b,\sigma} + c_{i,b,\sigma}^\dagger c_{i,a,\sigma}),$$

$$T_i^y = \frac{1}{2i}\sum_\sigma (c_{i,a,\sigma}^\dagger c_{i,b,\sigma} - c_{i,b,\sigma}^\dagger c_{i,a,\sigma}),$$

$$T_i^z = \frac{1}{2}\sum_\sigma (c_{i,a,\sigma}^\dagger c_{i,a,\sigma} - c_{i,b,\sigma}^\dagger c_{i,b,\sigma}). \tag{8}$$

For the present, we exploit the separation of spin and orbital Hilbert spaces and do not discuss the mixed-order parameters, though they are certain to be as relevant as $\mathbf{S}$ and $\mathbf{T}$ in high-symmetry situations. The symmetry classification

of the orbital-order parameters is obtained by representing the point group $\mathcal{D}_{3d}$ on the basis of the order parameters. In fact, since T^x, T^y, and T^z are composed as $c_\alpha^\dagger c_\beta$, the representation we seek is the product of the representation (1) and (2) with its adjoint, and the decomposition $E \otimes E = A_1 + A_2 + E$ can be used again. It turns out that T^x and T^z form the basis of the irrep E (a quadrupolar doublet), while T^y transforms according to A_2. We quote the transformation of the quadrupole operators under the $\mathcal{C}_3$ rotation

$$T'^x = -\frac{1}{2}T^x + \frac{\sqrt{3}}{2}T^z$$

$$T'^z = -\frac{\sqrt{3}}{2}T^x - \frac{1}{2}T^z. \tag{9}$$

From (1) it is clear that

$$\mathcal{C}_2 T^x = -T^x, \quad \mathcal{C}_2 T^y = -T^y, \quad \text{and} \quad \mathcal{C}_2 T^z = T^z. \tag{10}$$

Finally, let us mention that T_x and T_z are time-reversal invariant. The fact that under the time-reversal transformation $\mathcal{T}$, $\mathcal{T}T_x=T_x$ and $\mathcal{T}T_z=T_z$, shows that these are quadrupolar-order parameters. On the other hand, for the pure imaginary operator T^y, $\mathcal{T}T_y=-T_y$. In the usual treatment of a cubic e_g doublet, T^y would be an octupolar-order parameter. However, under trigonal symmetry, A_2 is also assigned to the dipolar-order parameter L_{111} (orbital angular momentum along the 111 direction). Thus our T^y must be a mixed dipolar-octupolar-order parameter, but we will not analyze its nature in detail.

The form of the effective pair interaction is restricted by the geometrical symmetries of the pair, and the nature of the order parameters (8). We consider a pair of sites 1 and 2 connected by the $\mathcal{C}_2$ axis, which figured in our previous considerations. The other symmetry element is the perpendicular mirror plane σ_h bisecting (1,2).

The orbital component of the lowest order effective Hamiltonian consists of terms $T_1^\alpha T_2^\beta$ ($\alpha,\beta=x,y,z$), and also of single-site terms like $T_1^\alpha + T_2^\alpha$ (reflecting that the choice of the basis is tied to this particular $\mathcal{C}_2$ axis). The pair energy expression must be invariant under $\mathcal{C}_2$, $\mathcal{T}$, and also σ_h. σ_h acts like

$$\sigma_h T_1^x = -T_2^x, \quad \sigma_h T_1^y = -T_2^y, \quad \text{and} \quad \sigma_h T_1^z = T_2^z. \tag{11}$$

Time-reversal invariance excludes terms like $T_1^x T_2^y$, and also $T_1^y + T_2^y$, and either (10) or (11) exclude $T_1^x + T_2^x$. In addition, (10) excludes also $T_1^x T_2^z$. Thus we are left with

$$\mathcal{H}_{12}' = A_x T_1^x T_2^x + \widetilde{A}_y T_1^y T_2^y + \widetilde{A}_z T_1^z T_2^z + A_z'(T_1^z + T_2^z), \tag{12}$$

where A_x, $\widetilde{A}_y$, $\widetilde{A}_z$, and A_z' are some real coefficients. Let us emphasize that, in general, the coupling term $T_1^y T_2^y$ may appear in the Hamiltonian. Once we introduce spins in the problem, the same arguments hold as above, with or without spin exchange, so the Hamiltonian becomes

$$\mathcal{H}_{12} = A T_1^x T_2^x + \widetilde{A}_y T_1^y T_2^y + \widetilde{A}_z T_1^z T_2^z + A_z'(T_1^z + T_2^z) + [B' + B T_1^x T_2^x$$
$$+ \widetilde{B}_y T_1^y T_2^y + \widetilde{B}_z T_1^z T_2^z + + B_z'(T_1^z + T_2^z)]\mathbf{S}_1\mathbf{S}_2. \tag{13}$$
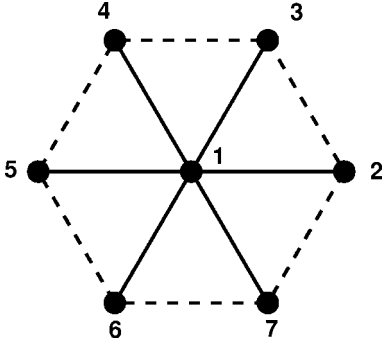
FIG. 3. The six neighbors of site 1.

Now we consider bonds with different orientation. Lattice site 1 has six nearest neighbors 2, 3, 4, 5, 6, and 7, which form a regular hexagon (Fig. 3). The interaction energy must be the same for the pairs (1,2), (1,3), etc., but just for this reason, the form of the pair Hamiltonians cannot be. They have to be derived from $\mathcal{H}_{ij=12}$ by suitable transformations.

Consider first the (1,5) pair, which is the mirror image (either through a σ_h plane containing 1, or by inversion through site 1) of the (1,2) pair. We can use (11) to deduce $T_2^x \rightarrow -T_5^x$, $T_2^y \rightarrow -T_5^y$, and $T_2^\xi \rightarrow T_5^\xi$, thus $\mathcal{H}_{ij=15}$ is of the same form as $\mathcal{H}_{ij=12}$. The (1,4) pair interaction can be deduced by the $\mathcal{C}_3$ rotation [Eq. (9)] from Eq. (13). In fact,

$$T_1^x \rightarrow -\frac{1}{2}T_1^x + \frac{\sqrt{3}}{2}T_1^\xi, \quad T_2^x \rightarrow -\frac{1}{2}T_4^x + \frac{\sqrt{3}}{2}T_4^\xi$$

$$T_1^\xi \rightarrow -\frac{\sqrt{3}}{2}T_1^x - \frac{1}{2}T_1^\xi, \quad T_2^\xi \rightarrow -\frac{\sqrt{3}}{2}T_4^x - \frac{1}{2}T_4^\xi, \quad (14)$$

which is more conveniently written as

$$\mathbf{T}_1 \rightarrow \mathbf{n}_{14} \cdot \mathbf{T}_1 \quad \mathbf{T}_2 \rightarrow \mathbf{n}_{14} \cdot \mathbf{T}_4 \quad (15)$$

with

$$\mathbf{n}_{14} = \begin{pmatrix} -\frac{1}{2} & 0 & \frac{\sqrt{3}}{2} \\ 0 & 1 & 0 \\ -\frac{\sqrt{3}}{2} & 0 & -\frac{1}{2} \end{pmatrix}$$

and the column vector $\mathbf{T} = (T^x, T^y, T^\xi)$. Similarly,

$$\mathbf{n}_{15} = \begin{pmatrix} -1 & 0 & 0 \\ 0 & -1 & 0 \\ 0 & 0 & 1 \end{pmatrix}.$$

For pairs of different orientation [e.g., (1,3)], analogous expressions can be given. For the pair ij, the effective Hamiltonian $\mathcal{H}_{ij}$ could be deduced from (13) by replacing $T^\alpha \rightarrow (\mathbf{n}_{ij}\mathbf{T})^\alpha = \mathbf{n}_{ij}^\alpha \mathbf{T}$ everywhere, where the $\mathbf{n}_{ij}^\alpha$ with $\alpha = x, y, z$ denotes the first, second, or third row of matrix $\mathbf{n}_{ij}$, respectively. However, it is worth noting the following simplification. Under these transformations $T_1^y T_2^y \rightarrow T_i^y T_j^y$ and $T_1^x T_2^x + T_1^\xi T_2^\xi \rightarrow T_i^x T_j^x + T_i^\xi T_j^\xi$. In other words, the orbital base-changing transformations have the character of a rotation

about the pseudospace y axis. Pseudospin-space symmetry is easier to identify if in the first line of Eq. (13) we make the following rearrangement:

$$A T_i^x T_j^x + \tilde{A}_y T_i^y T_j^y + \tilde{A}_z T_i^\xi T_j^\xi$$

$$= A\mathbf{T}_i\mathbf{T}_j + (\tilde{A}_y - A)T_i^y T_j^y + (\tilde{A}_z - A)T_i^\xi T_j^\xi$$

$$= A\mathbf{T}_i\mathbf{T}_j + A_y T_i^y T_j^y + A_z T_i^\xi T_j^\xi. \quad (16)$$

$\mathbf{T}_i\mathbf{T}_j$ and $T_i^y T_j^y$ are invariant, so from the intersite interaction terms, only the coefficient of the $T_i^\xi T_j^\xi$ term depends on the orientation of the pair. The effective pair Hamiltonian is then:

$$\mathcal{H}_{ij} = [A\mathbf{T}_i\mathbf{T}_j + A_y T_i^y T_j^y + A_z(\mathbf{n}_{ij}^z\mathbf{T}_i)(\mathbf{n}_{ij}^z\mathbf{T}_j) + A_z'(\mathbf{n}_{ij}^z\mathbf{T}_i + \mathbf{n}_{ij}^z\mathbf{T}_j)]$$

$$+ [B' + B\mathbf{T}_i\mathbf{T}_j + B_y T_i^y T_j^y + B_z(\mathbf{n}_{ij}^z\mathbf{T}_i)(\mathbf{n}_{ij}^z\mathbf{T}_j)$$

$$+ B_z'(\mathbf{n}_{ij}^z\mathbf{T}_i + \mathbf{n}_{ij}^z\mathbf{T}_j)]\mathbf{S}_i\mathbf{S}_j. \quad (17)$$

For completeness, we list here $\mathbf{n}_{ij}^z$ in all the six possible directions:

$$\mathbf{n}_{12}^z = \mathbf{n}_{15}^z = (0,0,1) \quad (18)$$

$$\mathbf{n}_{13}^z = \mathbf{n}_{16}^z = \left(\frac{\sqrt{3}}{2}, 0, -\frac{1}{2}\right) \quad (19)$$

$$\mathbf{n}_{14}^z = \mathbf{n}_{17}^z = \left(-\frac{\sqrt{3}}{2}, 0, -\frac{1}{2}\right). \quad (20)$$

The lattice Hamiltonian

$$\mathcal{H} = \sum_{\langle i,j \rangle} \mathcal{H}_{ij} \quad (21)$$

is the sum of (17) over all nearest-neighbor pairs. In the summation the A_z' coefficient drops out as $\mathbf{n}_{12}^z\mathbf{T}_1 + \mathbf{n}_{14}^z\mathbf{T}_1 + \mathbf{n}_{16}^z\mathbf{T}_1 = 0$. The Hamiltonian above contains pure orbital couplings, pure Heisenberg spin exchange, and also terms of coupled spin-orbital character. The only symmetries of the lattice Hamiltonian are global SU(2) for the spins and the space group symmetry.

We note here that our theory can be applied to any triangular d^1 system whose local Hilbert space is the trigonal doublet E. The structure of $BaVS_3$ can be envisaged as the sequence of triangular planes of $V^{4+} = 3d^1$ ions. It has been argued that even the minimal model of $BaVS_3$ should include the orbital degrees of freedom.[25] If one assumes that the lowest-lying crystal field level is the E doublet derived from the trigonal splitting of t_{2g}, our present considerations become relevant for $BaVS_3$ as well.

D. Effective Hamiltonian from microscopic model

Symmetry considerations do not allow us to obtain relationships between the A and B coefficients; they may be derived from the model (3) and (7) by second-order large-U perturbation theory, as usual for Kugel–Khomskii Hamiltonians.[16] As a result, we get

$$\mathcal{H}_{ij} = -\frac{2}{\tilde{U} + 2J_p}\Bigg[2tt'\mathbf{T}_i\mathbf{T}_j - 4tt'T_i^yT_j^y + (t-t')^2(\mathbf{n}_{ij}^z\mathbf{T}_i)(\mathbf{n}_{ij}^z\mathbf{T}_j)$$

$$+ \frac{1}{2}(t^2 - t'^2)(\mathbf{n}_{ij}^z\mathbf{T}_i + \mathbf{n}_{ij}^z\mathbf{T}_j) + \frac{1}{4}(t^2 + t'^2)\Bigg]\mathcal{P}_{ij}^{S=0}$$

$$- \frac{2}{\tilde{U}}\Bigg[4tt'T_i^yT_j^y + \frac{1}{2}(t^2 + t'^2) + \frac{1}{2}(t^2 - t'^2)$$

$$\times(\mathbf{n}_{ij}^z\mathbf{T}_i + \mathbf{n}_{ij}^z\mathbf{T}_j)\Bigg]\mathcal{P}_{ij}^{S=0} - \frac{2}{\tilde{U} - J_H}\Bigg[-2tt'\mathbf{T}_i\mathbf{T}_j$$

$$- (t-t')^2(\mathbf{n}_{ij}^z\mathbf{T}_i)(\mathbf{n}_{ij}^z\mathbf{T}_j) + \frac{1}{4}(t^2 + t'^2)\Bigg]\mathcal{P}_{ij}^{S=1}. \qquad (22)$$

We found it convenient to express the Hamiltonian using the $\mathcal{P}_{ij}^{S=0}$ and $\mathcal{P}_{ij}^{S=1}$ projection operators onto the singlet and triplet spin combination on the bond

$$\mathcal{P}_{ij}^{S=0} = \frac{1}{4} - \mathbf{S}_i\mathbf{S}_j \quad \text{and} \quad \mathcal{P}_{ij}^{S=1} = \mathbf{S}_i\mathbf{S}_j + \frac{3}{4}. \qquad (23)$$

First, some general remarks about the parameter range. Equation (7) shows a two-parameter manifold of on-site Coulomb Hamiltonians. However, we do not change J_p/J_H continuously, but investigate two special cases only: (a) neglecting pair hopping $J_p=0$ (a frequent, though not clearly motivated, simplification), and (b) the physically motivated choice $J_p=J_H/2$. Most of our results will be about the latter case, using the notation $J=2J_p=J_H$.

Redefining the basis states $\phi_a \leftrightarrow \phi_b$ interchanges the definitions of t and t', thus it is sufficient to consider the $|t| > |t'|$ case. It is, however, worth noting that the orbital part of (22) becomes SU(2) invariant for $t=t'$ and $J_p=0$:

$$\mathcal{H}_{ij} = \frac{4t^2}{\tilde{U}}\left(\mathbf{T}_i\mathbf{T}_j + \frac{3}{4}\right)\left(\mathbf{S}_i\mathbf{S}_j - \frac{1}{4}\right) + \frac{4t^2}{\tilde{U} - J_H}\left(\mathbf{T}_i\mathbf{T}_j - \frac{1}{4}\right)$$

$$\times\left(\mathbf{S}_i\mathbf{S}_j + \frac{3}{4}\right). \qquad (24)$$

The lattice Hamiltonian has now global SU(2) symmetry for the spins and global SU(2) symmetry for the pseudospins [global SU(2)⊗SU(2), with the six conserved quantities $\Sigma_j S_j^\alpha$, $\Sigma_j T_j^\beta$, for $\alpha,\beta=x,y,z$].

A still higher symmetry is obtained for $J_H=J_p=0$ when the pair Hamiltonian simplifies to the SU(4) symmetrical[23]

$$\mathcal{H}_{ij} = \frac{8t^2}{\tilde{U}}\left(\mathbf{T}_i\mathbf{T}_j + \frac{1}{4}\right)\left(\mathbf{S}_i\mathbf{S}_j + \frac{1}{4}\right). \qquad (25)$$

The corresponding lattice Hamiltonian possesses global SU(4) symmetry (there are 15 conserved quantities: $\Sigma_j S_j^\alpha$, $\Sigma_j T_j^\beta$, and $\Sigma_j S_j^\alpha T_j^\beta$ for $\alpha,\beta=x,y,z$).

III. GROUND STATES OF THE PAIR AND TETRAHEDRON PROBLEMS

In what follows, we seek to find the possible different types of ground state of (21) on the triangular lattice. For a

first orientation, we describe the results for small systems, then go over to larger ones. Whenever possible, we use preconception-free numerical methods and then try to reinterpret the results with approximate theories that can, in principle, be generalized to infinite-system size. It is a general trend that with increasing system size, complicated states are found whose existence could not have been guessed by simple-minded extrapolation from small systems. Therefore we will have to be cautious in drawing conclusions about the thermodynamic limit.

Before we turn to the physically motivated $J_p=J_H/2$ case, we examine the case when the pair hopping amplitude is absent.

A. Two-site problem

For simple spin models, the correlations found for a pair of sites allow us to infer the character of the ordered phase in the thermodynamic limit.[26] Our first aim is to map the pair solutions and try to deduce how spin and orbital order may complement each other.

The most notable consequence of setting $J_p=0$ is that the $4tt'T_i^yT_j^y$ term cancels from the first and second row of the effective Hamiltonian (22). Naturally, there is still a $T_i^yT_j^y$ interaction included in the isotropic term $\mathbf{T}_i\mathbf{T}_j$. On this basis, one may not expect a preference for T^y-polarized (complex) orbital ground states. However, one should not overlook the possibility that the system may choose T^y-polarization as a compromise when interaction terms preferring real orbital order mutually frustrate each other.[27]

Let us note that the Hamiltonian of the $ij=12$ bond

$$\mathcal{H}_{12} = -\frac{2}{\tilde{U}}\Bigg[2tt'(T_1^xT_2^x + T_1^yT_2^y) + (t^2 + t'^2)T_1^zT_2^z + (t^2 - t'^2)$$

$$\times(T_1^z + T_2^z) + \frac{3}{4}(t^2 + t'^2)\Bigg]\mathcal{P}_{12}^{S=0} - \frac{2}{\tilde{U} - J_H}\Bigg[-(t^2 + t'^2)$$

$$\times T_1^zT_2^z - 2tt'(T_1^xT_2^x + T_1^yT_2^y) + \frac{1}{4}(t^2 + t'^2)\Bigg]\mathcal{P}_{12}^{S=1} \qquad (26)$$

has two additional symmetries characteristic of the two-site problem. One of them is axial symmetry about T^z in pseudospin space,[28] which allows us to classify the eigenstates as $T_1^z + T_2^z$ eigenstates. The other is the $t' \leftrightarrow -t'$ symmetry: a π-rotation about T^z in pseudospin space for site 2 is a canonical transformation that leaves the energy unchanged, but it amounts to $t' \to -t'$. This symmetry can be restated for larger clusters with bipartite structure, but it cannot be extended to $N>2$ clusters of the triangular lattice.

For $t=t'$ SU(2)⊗SU(2) symmetry follows as in (24). Taken in conjunction with the previous remarks, the $t=-t'$ model must have the same symmetry. Similarly, the degeneracies must be the same for the SU(4) point $t=t'$, $J_H=0$, and its mirror image $t=-t'$, $J_H=0$.

The Hilbert space of two electrons on two sites is 16 dimensional, and the energies and orbital eigenstates for the $ij=12$ bond are:
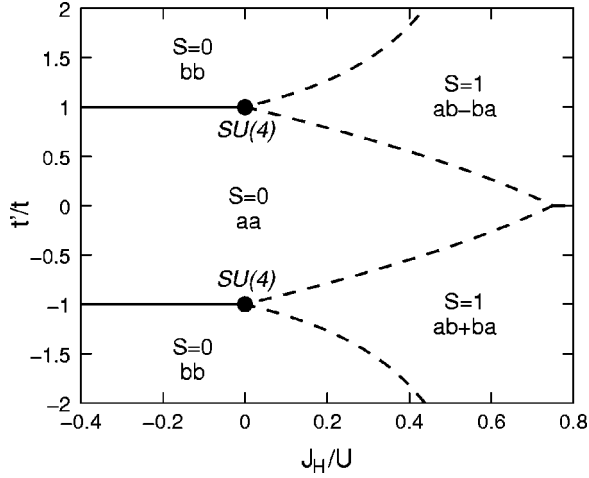
FIG. 4. Zero temperature phase diagram of the model on two sites as a function of t'/t and $J_H/\tilde{U}$. We have indicated the spin and orbital parts. Along the thick line at $t'/t=1$ and $J_H<0$ the ground state is triply degenerate: the orbital part becomes SU(2) symmetric, and the orbital triplet $|aa\rangle$, $|ab\rangle+|ba\rangle$ and $|bb\rangle$ with the spin singlet forms the ground-state wave function. Along the $t'/t=-1$ and $J_H<0$ line, the orbital triplet consists of $|aa\rangle$, $|ab\rangle-|ba\rangle$, and $|bb\rangle$. At the SU(4) points the ground state is 6-fold degenerate.

$$E_{S=0} = -\frac{4t^2}{\tilde{U}}, \quad E_{S=1}=0, \quad |aa\rangle$$

$$E_{S=0} = -\frac{4t'^2}{\tilde{U}}, \quad E_{S=1}=0, \quad |bb\rangle$$

$$E_{S=0} = -\frac{(t+t')^2}{\tilde{U}}, \quad E_{S=1}=-\frac{(t-t')^2}{\tilde{U}-J_H}, \quad |ab\rangle+|ba\rangle$$

$$E_{S=0} = -\frac{(t-t')^2}{\tilde{U}}, \quad E_{S=1}=-\frac{(t+t')^2}{\tilde{U}-J_H}, \quad |ab\rangle-|ba\rangle.$$

$$(27)$$

The results are shown in Fig. 4. Inside any of the ground-state phases, either the spins are parallel and the orbitals antiparallel, or vice versa. At the boundaries, the ground-state level has higher degeneracy, which can be interpreted as the manifestation of one of the higher symmetries discussed above.

For the spin singlets, $t \neq t'$ acts like an external orbital field, and therefore, orbital polarization is either in the a or the b direction. At the line $t=t'$ (section $J_H<0$) not only aa and bb (states from the neighboring domains) becomes degenerate but also $|ab\rangle+|ba\rangle$, thus the ground state is the threefold degenerate spin-singlet–orbital-triplet ($S=0$, $T=1$), allowed by the symmetry SU(2)⊗SU(2). Continuing the $t=t'$ line[29] to $J_H>0$, the ground state is again threefold degenerate, but its nature changed to spin-triplet–orbital-singlet ($|ab\rangle-|ba\rangle$). The border point $t=t'$, $J_H=0$ is the SU(4) point

where the ($S=0$, $T=1$), and ($S=1$, $T=0$) levels become degenerate [forming the basis of the 6D antisymmetrical irrep of SU(4)].

Analogous results hold for the other SU(2)⊗SU(2) line $t=-t'$, only for $J_H>0$, the $|ab\rangle-|ba\rangle$ orbital state ($T=0$, $T^z=0$) is changed to $|ab\rangle+|ba\rangle$ ($T=1$, $T^z=0$). Note that the energy difference between these two states comes from the term of (26) proportional to $t'(T_1^+T_2^-+T_1^-T_2^+)$, so changing the sign of t' changes the parity of the ground state. The sixfold degeneracy of the ground state at the "anti-SU(4)" point $t=-t'$, $J_H=0$ follows from the $t' \leftrightarrow -t'$ symmetry of the pair problem. A very similar phase diagram would be obtained for $J_p \neq 0$. We do not show it here, but we include the contribution of pair hopping in all our subsequent calculations.

If any far-reaching conclusions from Fig. 4 could be drawn, it would be that the ground state has either ferro-orbital order and spin antiferromagnetism (or a singlet spin liquid); or it is a spin ferromagnet with staggered orbital order (or orbital liquid). Less obviously, at the SU(4) points, a spin-orbital quantum liquid may be inferred.[15]

To either confirm or disprove these guesses, two routes can be followed: (a) determine the exact phase diagram of larger clusters and see if there is a clear trend emerging; (b) construct variational wave functions that possess the envisaged correlations. Figure 4 suggests that antiferromagnetic effective spin models can be derived easily because uniform orbital order factorizes site by site. However, for high-spin states, the orbital states are more complicated. SU(4)-like states, for which spins and orbitals are entangled, pose further challenge.

B. Four-site problem

In what follows, we set $J=2J_p=J_H$. The four-site cluster with periodic boundary conditions is equivalent to a tetrahedron, where the three directions on the triangular lattice correspond to the three pairs of opposite bonds on the tetrahedron. This cluster proves to be sufficiently large to provide us with some insight into the problem.

As a first step, we do exact (numerical) diagonalization for the Hamiltonian

$$\mathcal{H}_{\text{tetr}} = \mathcal{H}_{12} + \mathcal{H}_{13} + \mathcal{H}_{14} + \mathcal{H}_{23} + \mathcal{H}_{24} + \mathcal{H}_{34} \quad (28)$$

in the $4^4=256$-dimensional Hilbert space. The total spin S and its z-component S^z are good quantum numbers, but this is only of limited use in identifying eigenstates. The Hamiltonian couples spin correlations with orbital correlations, therefore, most of the eigenstates have mixed spin-orbital character. More precisely, the $S=2$ eigenstates can be sought in the factorized form

$$|\uparrow \uparrow \uparrow \uparrow\rangle \otimes \Phi(T_1,T_2,T_3,T_4),$$

but this is no longer true of lower-spin states. In particular, we know that there are only two independent spin singlet states, [12][34] and [23][41], but combined with the orbitals, we have 32 independent $S=0$ spin-orbital states. Most of the $S=0$ eigenstates of Eq. (28) are not represented as a linear combination of the above singlets multiplied by a pure orbital state. In fact, an overall singlet which plays a prominent
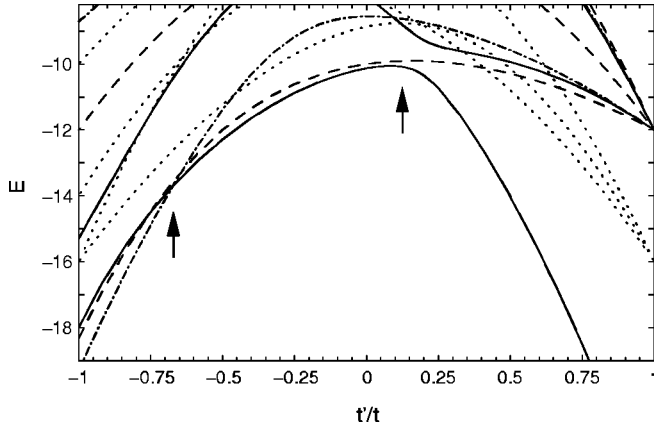
FIG. 5. Energy spectrum of the spin singlet sector in the tetrahedron as a function of t'/t for the $J_H=J_p=0$ case. For t'/t between 0.2 and 1 the ground state is well separated from the rest of the states, and it is the adiabatic continuation of the SU(4) singlet state at the $t'/t=1$ point (full line). The SU(4) singlet nature of the ground state is lost at around $t'/t=0.2$ (denoted by an arrow), and in the region $-0.7 < t'/t < 0.2$ three levels [a non-degenerate level (solid line) and a two-fold degenerate level (dashed line)] go together. Finally, at $t'/t=-0.7$ the symmetry of the ground state changes, indicating the appearance of the third phase (dashed-dotted line).

role in our considerations is the SU(4) plaquette singlet

$$\Psi_{SU(4)} = [12]\{23\}[34]\{41\} - [23]\{34\}[41\}\{12\} \quad (29)$$

where $\{23\}$ represents the pseudospin singlet connecting sites 2 and 3, etc. It is clear that $\Psi_{SU(4)}$ is a spin singlet, just as it is a pseudospin singlet, and it does not factorize in spin and orbital variables. $\Psi_{SU(4)}$ is the ground state of $\mathcal{H}_{tetr}$ in the SU(4)-symmetrical point ($t=t'$, $J=0$) of the parameter space of (28). It is the only SU(4) singlet [the only basis function for the 1-dim irrep of SU(4)] in the present Hilbert space.

We diagonalized (28), and followed the low-lying states (a representative example is shown in Fig. 5). While the detailed nature of the ground state always has some continuous dependence on the Hamiltonian parameters t'/t and J/U, there are also sharp changes at level crossings. A level crossing is possible between states with different symmetry labels. The symmetry of $\mathcal{H}_{tetr}$ is $SU(2) \otimes T_d$, where T_d is the tetrahedral group. T_d has 1D and 3D irreps; furthermore, granting time-reversal invariance, two complex conjugate 1D irreps belong to degenerate energy levels. We distinguish between ground states according to their spin degeneracy ($2S+1$), and orbital degeneracy, which can be 1, 2, or 3.

The resulting phase diagram is shown in Fig. 6. Phase boundaries were drawn where we found a clear change in the character of the ground state; this holds also for the boundary between the two nondegenerate ($S=0$, 1x) phases. Let us immediately point out that the tetrahedral phase diagram is very different, and therefore would have been difficult to guess, from the pair phase diagram shown in Fig. 4. Taken in itself, the lack of mirror symmetry about the $t'=0$ axis was to be expected, since the tetrahedral cluster is not bipartite. In particular, the $t'=-t$, $J_H=0$ point does not have any special
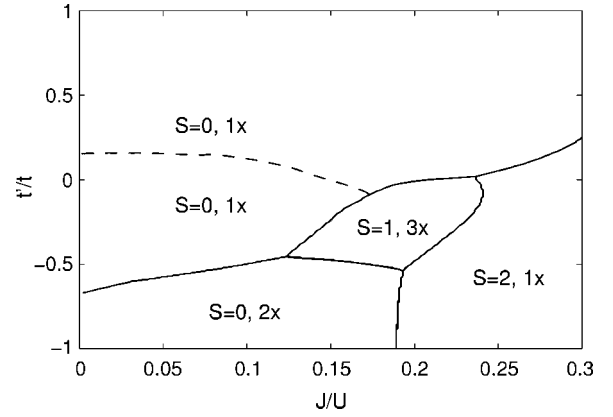
FIG. 6. Phase diagram of the spin-orbital model with $J=J_H=2J_p$ and $U=\tilde{U}-J$ on a tetrahedron, based on exact diagonalization (see also Fig. 5). Phase boundaries in bold lines belong to level crossings in the ground state energy. A further singlet-to-singlet transition is identified in the vicinity of an antilevel crossing (dashed line). The degeneracy (apart from the trivial spin degeneracy) of each state is also indicated.

significance. However, less obvious features are the variety of singlet phases, the shrinking of the domain of spin-polarized solutions, and the predominance of the singlet phase into which the SU(4) point is embedded.

IV. VARIATIONAL APPROACH FOR THE FOUR-SITE CLUSTER

A. The method

The previous section showed us that we could expect a rich phase diagram for our model even on a small-size cluster. We will continue our investigation by studying larger clusters by a kind of variational method: since there is a strong asymmetry between the spin and the orbital parts in the Hamiltonian, we try to decouple spin and orbital degrees of freedom[30] by factorizing the wave function into a $|\Psi^S\rangle$ spin and $|\Psi^T\rangle$ orbital part:

$$|\Psi_{ST}\rangle = |\Psi^S\rangle \otimes |\Psi^T\rangle. \quad (30)$$

While this factorization applies to the pair problem, it cannot describe the entanglement of spin and orbital fluctuations for $N \geq 4$ sites. In particular, it does not allow us to capture the SU(4) character displayed by (29). However, it should work well for states with weakly fluctuating orbital order.

We proceed as follows: in the effective Hamiltonian we can separate a spin-orbital mixing term from purely orbital terms:

$$H = \sum_{i,j} \{2(\mathbf{S}_i \cdot \mathbf{S}_j)\mathbf{h}_{ij}^{\mathbf{T}} + \mathbf{k}_{ij}^{\mathbf{T}}\}. \quad (31)$$

Next, we need to minimize the Hamiltonian by using the factorized wave function: $\langle\Psi_{ST}|H|\Psi_{ST}\rangle$. It implies that $|\Psi_S\rangle$ is an eigenstate of the Hamiltonian

$$\sum_{i,j} 2(\mathbf{S}_i \cdot \mathbf{S}_j)\langle\Psi_T|h_{ij}^T|\Psi_T\rangle \quad (32)$$

while $|\Psi_T\rangle$ is an eigenstate of the Hamiltonian
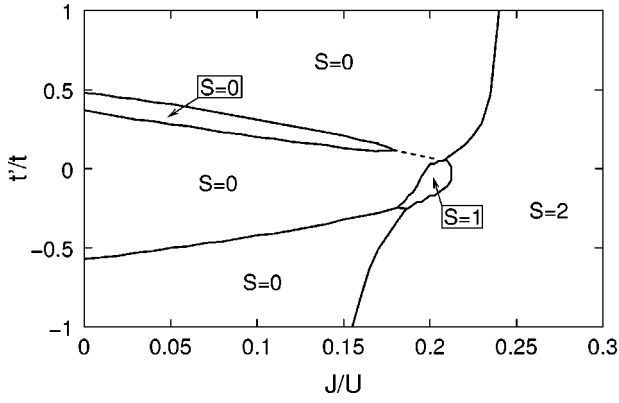
FIG. 7. The phase diagram of the effective model on a tetrahedron based on the spin-orbital decoupling scheme (30).

$$\sum_{i,j} (2\langle\Psi_S|\mathbf{S}_i\mathbf{S}_j|\Psi_S\rangle h_{ij}^T + k_{ij}^T). \tag{33}$$

This coupled set of equations is solved by iteration, keeping at each step the solutions with lowest eigenvalue. We have applied this technique to obtain the phase diagram of the regular four-site (tetrahedron) and 16-site cluster.

B. Phase diagram on a tetrahedron

As we can see in Fig. 7, the "mean-field" phase diagram shows a remarkable resemblance to the exact one (Fig. 6). We should, however, note that the ferromagnetic region extended too much at the expense of the SU(4) phase, basically because the Ansatz (30) cannot describe SU(4) correlations,[31] while the spin-aligned states are treated correctly. The $S=1$ region has shrunk, too. Our variational recipe for $S=1$ states is to compose them of two bonds: a spin triplet and orbital $|ab\rangle+|ba\rangle$ bond, and a spin singlet and orbital $|aa\rangle$ type bond. These can be permuted and rotated to give six solutions that are degenerate at the mean-field level. Allowing for the resonance between these six states, we can reproduce the 3-fold degenerate $S=1$ state seen in the exact-digonalization study by taking the appropriate linear combinations of them.

In the singlet sector we can distinguish between several phases: the lowest one is composed of spin triplet and orbital $|ab\rangle+|ba\rangle$-like bonds, which are composed into a singlet, and is threefold degenerate at the mean-field level due to possible rotations (here again, the off diagonal matrix elements between the states will favor the twofold degenerate linear combination, in agreement with Fig. 6). In the remaining part, the spin wave functions is the same (singlet valence bonds), only the orbital character changes from $|aa\rangle$ type bonds to a more complicated one close to the $t=t'$, $J=0$ SU(4)-symmetric point (where the approach we use is clearly not applicable). The number of solutions of the iteration becomes very large in the vicinity of the SU(4) point, with essentially the same energy.

V. VARIATIONAL APPROACH FOR THE 16-SITE CLUSTER

The tetrahedron solutions show that there must be quite a few phases with markedly different spin-orbital correlations.
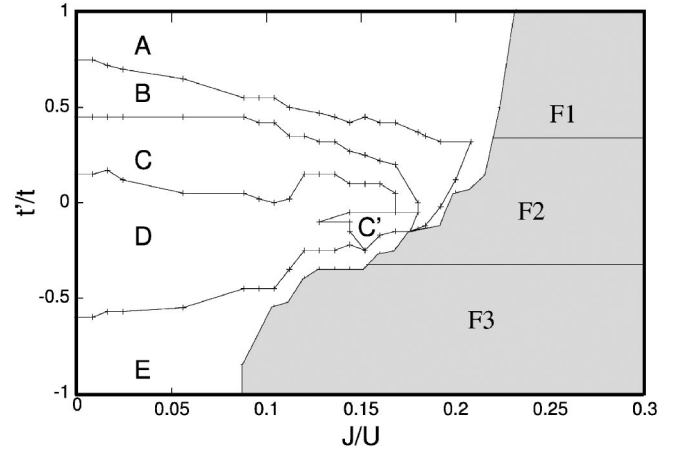
FIG. 8. Mean-field phase diagram on a 16-site cluster as a function of hopping integral versus Hund's coupling. The grey phase is the ferromagnetic phase, with the classical phase boundaries shown (see Sec. V B).

However, the $N=4$ cluster is too small to draw inferences about the character of any emerging long-range order (except for spin ferromagnetism). Therefore, we investigated an $N=16$ cluster that is large enough to differentiate between quasi-1D (chains) and genuinely 2D orbital ordering patterns. We use the same variational method as for $N=4$.

As shown in Fig. 8, the model leads to a rich phase diagram. For reasonably large values of J/U we find the fully polarized ferromagnetic ($S=8$) region with three phases that differ by their orbital structure. In the spin singlet region we can again distinguish at least six phases, which are labeled by capital letters. A detailed discussion of these phases follows.

A. Singlet phases

The $S=0$ part of the diagram is composed of six phases. We have investigated in more detail each phase starting from $t'/t\sim-1$ and going through the four boundaries until $t'/t\sim1$ for several ratios J/U. The aim of this section is to understand the different types of orbital and spin orders. The nature of the spin phases turned out to be easily determined from the variational method itself: In all cases except phase A, some clear pattern with large and positive or negative values of $\langle\mathbf{S}_i\cdot\mathbf{S}_j\rangle$ could be identified, leading to magnetic or singlet dimer order. The orbital part was more tricky to identify since the most relevant operator is not $\mathbf{T}_i\cdot\mathbf{T}_j$ but h_{ij}^T, and a given mean-value of this parameter does not obviously lead to an orbital state since this operator is quite involved. So to get a simple physical picture of the orbital structure we have tried in each case to reproduce the pattern given by the mean-field solution for $\langle h_{ij}^T\rangle$ assuming at each site an orbital wave function of the form

$$|\Psi_i^T\rangle = (\cos\,\theta_i|a_i\rangle + \sin\,\theta_i|b_i\rangle) \tag{34}$$

and we have checked that this orbital structure also reproduces satisfactorily the mean value of $\mathbf{T}_i\cdot\mathbf{T}_j$ measured in the mean-field ground state. This turned out to give a clear pic-
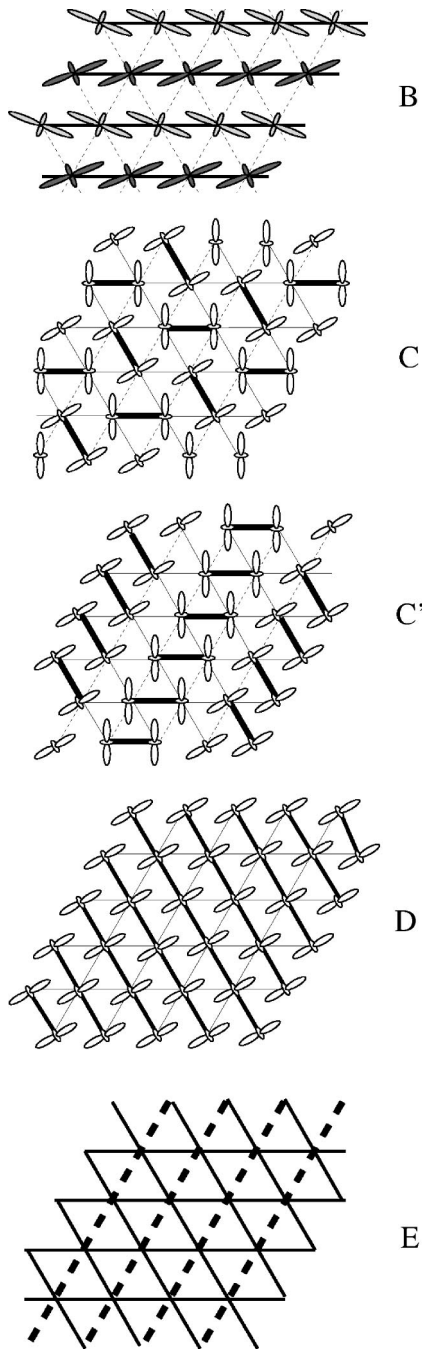
FIG. 9. Spin and orbital structure in the singlet phases of the mean-field phase diagram. Solid line indicates AF, dashed line FM spin correlations.

ture in all phases except A and E. The information obtained in this way is summarized in Fig. 9. In the following, we describe in more detail all these phases.

1. Phase A

This phase contains the SU(4) point ($t'=t$, $J=0$) for which the mean-field decoupling used here is known to be inadequate given the very symmetric roles played by the spin and orbital degrees of freedom.[32] In fact, it is believed that at the SU(4) point the system is in a spin-and-orbital liquid

state involving resonances between SU(4) singlet plaquettes. A discussion of the physical properties at the SU(4) point can be found in Ref. 15. Although the mean-field solution is not directly relevant for that phase, the mean-field approach is still useful to determine the boundary of the SU(4) region since it allows us to detect the domain of stability of the neighboring phases, for which the mean-field solution is indeed relevant, as will be discussed later. As anticipated, the SU(4) physics extends to a finite and relatively large portion of the phase diagram, and it can in principle be relevant for real systems. Since our mean-field approach does not lead to any physical insight beyond the determination of the boundary of this phase, however, we will not discuss it further here.

2. Phase B

From the magnetic point of view, this phase consists essentially of weakly coupled, antiferromagnetic chains (see Fig. 9), while the orbital structure turns out to be rather subtle with an antiferro-orbital arrangement of ferro-orbital chains with orbitals that are neither pure $|a\rangle = |d_{3z^2-r^2}\rangle$ nor $|b\rangle = |d_{x^2-y^2}\rangle$ but alternate between $1/\sqrt{2}(|a\rangle+|b\rangle)$ and $1/\sqrt{2}(-|a\rangle+|b\rangle)$. The detailed magnetic structure depends *a priori* on the residual couplings between the chains. If the couplings are equal in both residual directions, some canting will presumably develop inside the chains to accomodate the frustration, like in the limiting case of the 120° classical ground state of the Heisenberg model on the triangular lattice. This effective magnetic Hamiltonian would be similar to that realized in Cs_2CuCl_4, with possibly spinon excitations as reported by Coldea *et al.*[33] If, however, the symmetry is broken between the residual directions, the system is expected to develop rather collinear order, with lines of parallel spins along the direction of the most ferromagnetic or least antiferromagnetic residual coupling. For all parameters, the residual couplings predicted by the mean-field solution are very small, but their sign and symmetry depends on the parameters. They tend to be AF for small J and ferromagnetic for large J, and the symmetry between the two directions may or may not be broken depending on the parameters. While this interesting point would deserve further investigation, we do not think that a reliable answer to such a subtle issue can be obtained just on the basis of this mean-field decoupling, and we do not discuss the point further.

3. Phases C and C'

Both phases are characterized by strong dimer singlets forming different regular dimer coverings of the triangular lattice. On each dimer the orbitals are parallel, and they correspond to $d_{3z^2-r^2}$, $d_{3x^2-r^2}$, or $d_{3y^2-r^2}$ depending on the orientation of the bond. Note that all these orbitals are Jahn-Teller active, leading in all cases to two long bonds and four short bonds. One might be tempted to conclude that these phases correspond to two types of valence bond solids with the patterns depicted in Fig. 9. The mean-field approach has a very remarkable property, however. In addition to the mean-field solutions with lowest energy shown in Fig. 9, there are several other mean-field solutions of the self-consistent equa-

tions with energies very close to the lowest energy corresponding to other dimer coverings of the triangular lattice. In such circumstances, going beyond mean-field is likely to couple these solutions, and the relevant model would then be a quantum dimer model describing resonances between these states. As we shall see later, this point of view is favored by exact diagonalizations of finite clusters. So at that stage we think it is safer to think of these phases as a region of parameters where all dimer coverings are relevant states for low-energy physics.

4. Phase D

This phase consists essentially of weakly coupled antiferromagnetic chains, but in contrast to Phase B, the orbital structure is now ferro-orbital with only orbital $d_{3z^2-r^2}$, $d_{3x^2-r^2}$, or $d_{3y^2-r^2}$ depending on the overall direction of the AF chains. Since these orbitals are Jahn-Teller active, one expects in this case that the system would undergo a cooperative Jahn-Teller distortion with two long bonds per octahedra all pointing in the same direction. Like in Phase B, the actual magnetic structure will be controlled by the residual couplings, and all the discussion of Phase B applies here, including the sign of the residual couplings and the symmetry of the couplings in the directions of weak coupling. In that case too, a reliable determination of the possible magnetic phases requires further investigation that goes beyond the present mean-field calculation.

5. Phase E

This phase is dominated by strong antiferromagnetic correlations in two directions and weak ferromagnetic correlations in the third direction, leading to an effective Néel structure. The orbital structure cannot be reproduced satisfactorily with the variational ansatz of one orbital wave function per site. The pattern of $\langle h_{ij}^T \rangle$ would be consistent with a ferro-orbital ordering with orbitals $1/\sqrt{2}(|a\rangle+|b\rangle)$ at all sites, but the $\mathbf{T}_i \cdot \mathbf{T}_j$ correlations are not ferromagnetic. So to decide on a possible orbital order would require to go beyond the present mean-field approach.

B. Ferromagnetic phase

In the ferromagnetic region the $\mathcal{P}_{ij}^{S=0}$ spin singlet projection is 0, so that the effective Hamiltonian (22) is reduced to the following form (neglecting the constant term):

$$H_{\text{eff}}^{\text{FM}} = \frac{2}{\tilde{U} - J_H} \sum_{i,j} [(t-t')^2 (\mathbf{n}_{ij}^z \mathbf{T}_i)(\mathbf{n}_{ij}^z \mathbf{T}_j) + 2tt' \mathbf{T}_i \mathbf{T}_j]$$

(35)

and the orbital structure only depends on the ratio t'/t. As shown in the phase diagram 8 we can distinguish three phases going from $t'/t=-1$ to $t'/t=1$. All the identified phases identified are orbitally ordered phases. They can be understood starting from the classical limit, which in our case is equivalent to minimizing the energy of the
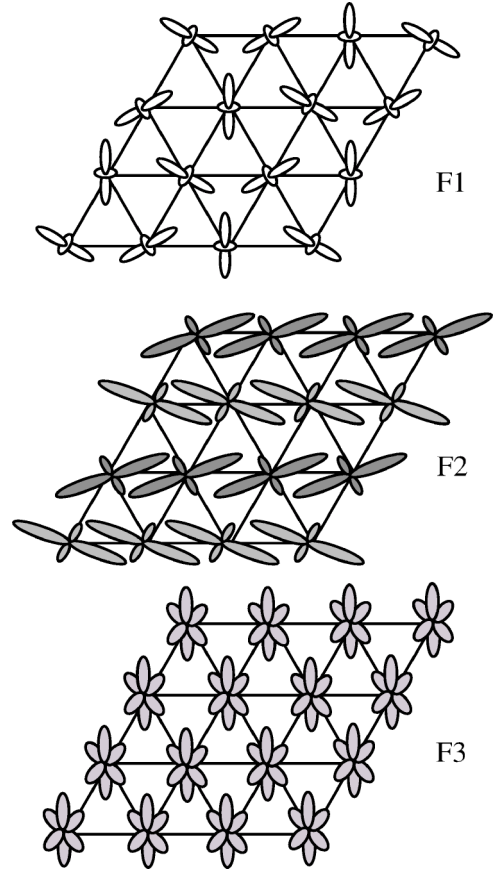
FIG. 10. Schematic representation of the orbital orderings in the spin ferromagnetic case.

$$|\Psi\rangle = \prod_j (\cos\,\theta_j |a\rangle + e^{i\phi_j}\sin\,\theta_j |b\rangle)$$

(36)

site-factorized wave function. The phase boundaries shown in Fig. 8 are obtained by equating classical energies obtained from the wave function of Eq. (36).

1. Phase F1

For $t'=t$ the Hamiltonian of the orbitals becomes the standard SU(2) symmetric Heisenberg Hamiltonian with antiferromagnetic exchange. In this case a three-sublattice long-range order (LRO) for the **T** pseudospins develops. Away from the SU(2) symmetric point, the three-sublattice LRO is stable up to $t'=t/3$, with the 120° configuration restricted in the (T^x, T^z) plane [in Eq. (36) we choose θ for θ_j's in the first, $\theta+2\pi/3$ for θ_j's in the second, and $\theta-2\pi/3$ for θ_j's in the third sublattice, with $\phi_j=0$ everywhere] with energy

$$\frac{E_{\text{AFO}}}{N} = -\frac{3}{8}\frac{(t+t')^2}{\tilde{U}-J_H}.$$

(37)

We have shown a possible 120° orbital pattern with $\theta=0$ in the top of Fig. 10. While the classical approach does not allow us to fix the value of θ, this degeneracy is probably lifted by quantum fluctuations.

For finite systems, the signature of the developing LRO can be found in the energy spectrum in the form of the
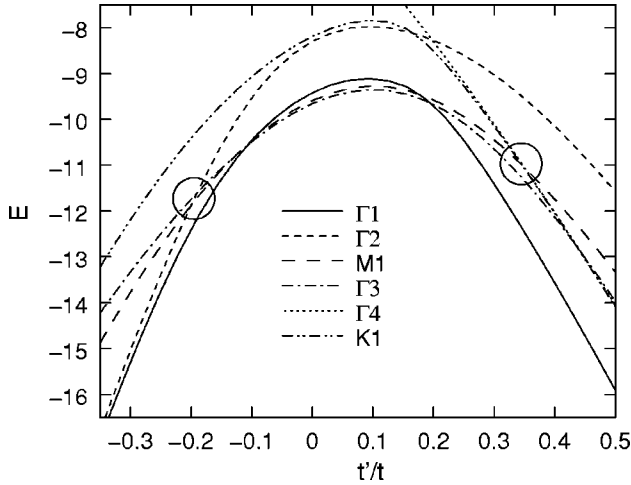
FIG. 11. Energy level scheme of a 12 site diamond-like cluster with periodic boundary conditions and compatible with the 3-sublattice LRO. Shown are the levels which can be associated with the ferro-orbital T^y order (denoted by $\Gamma 1$ and $\Gamma 2$), collinear phase ($\Gamma 1$, $M1$, and $\Gamma 3$) and the lowest states constituting the Anderson tower of the $120°$ antiferro-orbital phase ($\Gamma 1$, $K1$, and $\Gamma 4$). The first letter refers to the momentum of the state. We have encircled the level crossings that we used to determine the phase boundary ($t'/t=-0.20$ and $t'/t=0.35$).

Anderson's tower, as has been confirmed by Bernu, Lhuiller, and Pierre for the isotropic triangular lattice.[34] These low-lying states ($\Gamma 1$, $K1$, and $\Gamma 4$) can also be seen in Fig. 11, and they can be continuously followed up to the isotropic point $t'=t$, where they become the lowest lying pseudospin triplet excitations. Further evidence comes from the nearest- and next-nearest-neighbor $\langle \mathbf{T}_i \mathbf{T}_j \rangle$ correlations. There is a strong ferro-orbital correlation between a site and its second nearest-neighbors, e.g., $\langle \mathbf{T}_i \mathbf{T}_j \rangle \sim 0.19$ for $t'/t=0.8$.

2. Phase F2

To understand this phase, we start from the $t'=0$ case, where the Hamiltonian (35) is proportional to $2\Sigma_{\text{bonds}}(\mathbf{n}_{ij}^z \mathbf{T}_i) \times (\mathbf{n}_{ij}^z \mathbf{T}_j)$, which can conveniently be transformed to

$$\sum_{\text{bonds}} ([\mathbf{n}_{ij}^z(\mathbf{T}_i + \mathbf{T}_j)]^2 - (\mathbf{n}_{ij}^z \mathbf{T}_i)^2 - (\mathbf{n}_{ij}^z \mathbf{T}_j)^2)$$

$$= \sum_{\text{bonds}} [\mathbf{n}_{ij}^z(\mathbf{T}_i + \mathbf{T}_j)]^2 - 3\sum_i [(T_i^x)^2 + (T_i^z)^2]$$

$$= \sum_{\text{bonds}} [\mathbf{n}_{ij}^z(\mathbf{T}_i + \mathbf{T}_j)]^2 + 3\sum_i (T_i^y)^2 - 3NT(T+1).$$

At the classical level, the two squares can be minimized by choosing the $\mathbf{T}$ vector in the (T^x, T^z) plane so that on a given bond either $\mathbf{T}_i = -\mathbf{T}_j$, or $\mathbf{T}_i + \mathbf{T}_j$ is perpendicular to $\mathbf{n}_{ij}^z$. These conditions are satisfied with the collinear orbital order shown in Fig. 10, we choose $|a\rangle + |b\rangle$ along every second chain with the bond variable $\mathbf{n}_{ij}^z = (0,0,1)$, and $|a\rangle - |b\rangle$ along the remaining chains (the orbital configuration is the same as in phase B in Fig. 9). There are six such configurations, which can be obtained by translations and rotations, with variational energy

$$\frac{E_{\text{CL}}}{N} = -\frac{1}{4}\frac{3t^2 - 2tt' + 3t'^2}{\tilde{U} - J_H}. \tag{38}$$

The classical phase boundaries for this state are $t'/t=-1/3$ and $t'/t=1/3$.

In a finite system with periodic boundary conditions respecting the point group $\mathcal{D}_{3d}$ of the triangular lattice, the linear combination of the six states will produce a threefold degenerate state at the M point in the Brillouin zone (state $M1$ in Fig. 11), and three states at the Γ point, one nondegenerate and one twofold degenerate ($\Gamma 1$ and $\Gamma 3$ in Fig. 11, respectively). These states can clearly be recognized in the exact diagonalization spectrum of the 12-site cluster as the lowest-lying state for $-0.2t < t' < 0.35t$, well separated from the states with higher energy. The observation of the phase in the correlation function is nontrivial, as the ground state around $t'=0$ is twofold degenerate, and the applied exact diagonalization on a finite size cluster will result in a state with an arbitrary linear combination of them, which leads to a pattern difficult to interpret. It is, however, clear that there is no ferro-orbital order.

3. Phase F3

In this phase the T^y ferro-orbital order is established: for negative t' the $\mathbf{T}_i \mathbf{T}_j$ term in Eq. (35) becomes ferromagnetic, and the frustration in the T^x and T^z due to the $(\mathbf{n}_{ij}^z \mathbf{T}_i)(\mathbf{n}_{ij}^z \mathbf{T}_j)$ term will single out the T^y order. The particularity of the T^y ordering is that it breaks the time-reversal symmetry: either the $|a\rangle + i|b\rangle$ or the $|a\rangle - i|b\rangle$ combination orders. The ordering of complex orbitals has been searched for in the context of manganites, where it has been thought that they are favored by the isotropic-kinetic exchange. Indeed, the charge density of the $|a\rangle \pm i|b\rangle$ shows the trigonal symmetry, and the combination is Jahn-Teller inactive. The phase can be easily identified in the finite-size diagolization from the correlation function: spatially isotropic $T_i^y T_j^y > 0$ correlations are dominant. The mean-field variational energy of the ferro-orbital complex state is

$$\frac{E_{\text{FO}}}{N} = \frac{3tt'}{\tilde{U} - J_H} \tag{39}$$

and the phase is stable for $t'/t < -1/3$.

The determination of the phase boundaries is, however, not straightforward. As can be seen from the energy levels, the $\Gamma 1$ state is present in the "ground-state manifold" of all the ordered phases. Therefore we identified the phase boundaries by level crossings of the ground-state manifolds associated with each type of ordering, which agree reasonably well with the classical phase boundaries ($t'/t=\pm 1/3$). At these phase boundaries continuous degeneracies appear in the classical wave function, suggesting a gapless excitation spectrum at those points.

VI. EXACT DIAGONALIZATIONS

Due to the small number of conveniently exploitable symmetries in the problem [we have only the spin SU(2) symmetry], the size of the Hilbert space grows very rapidly with
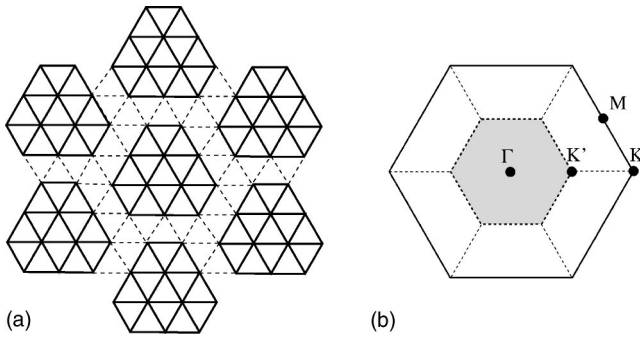
FIG. 12. The 12-site cluster with periodic boundary conditions, and the associated Brillouin zone.

the size. In the $S^z=0$ sector it increases like $\binom{N}{N/2}2^N$ where N is the number of sites. This limits us to small cluster sizes, especially if we want to explore the phase diagram. The obvious choice was the 12-site cluster with periodic boundary conditions (Fig. 12), which has the full $\mathcal{D}_{3d}$ symmetry of the lattice as well. The considered cluster has the advantage to allow the formation of SU(4) plaquettes and is also compatible with three- and four-sublattice order.

The phase diagram obtained from the level crossings in the ground state is shown in Fig. 13. It is globally consistent with the mean-field one. The fully polarized ferromagnetic region ($S=6$) is found for very similar values of J/U. For small J/U, we identify five different regimes from $t'/t=-1$ to $t'/t=+1$. They seem to correspond to four phases only, since two regions join for intermediate values of J/U, but given the difficulty to determine phase boundaries from exact diagonalizations, this should not be taken too seriously. The various regions are labeled according to the point in the Brillouin zone where the ground state is found.

In the vicinity of the SU(4)-point ($t'/t\sim1$, $J\sim0$), the low-lying spectrum is similar to the one obtained in the SU(4) case.[15] This suggests that the description of the ground state in terms of SU(4) singlets is applicable in this region.

At the M point the ground state is threefold degenerate. This could correspond to the formation of AF chains in
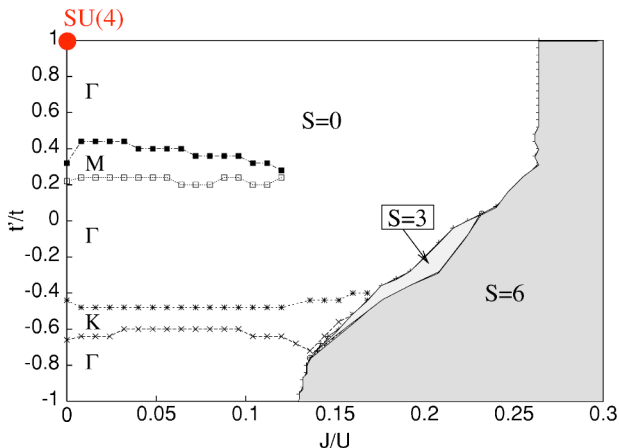
FIG. 13. Exact diagonalizations: phase diagram for the 12-site cluster.
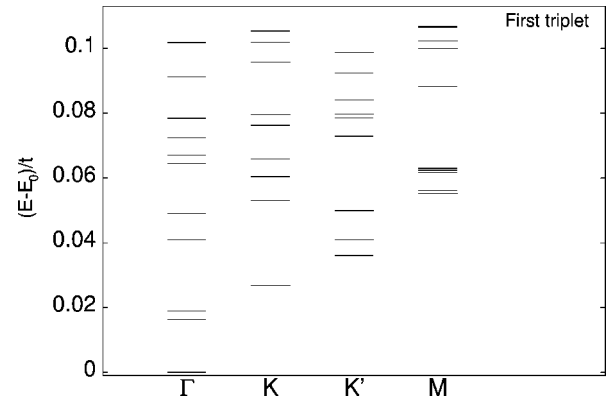
FIG. 14. Low-lying singlets for $t'/t=0$ and $J/U=0.008$.

phase B since these chains can form in three directions, resulting in a threefold degenerate mean-field solution. To confirm this interpretation, we have diagonalized the full Hamiltonian in the variational sub-space spanned by the mean-field ground state wave functions of Phase B. It turns out that these states are not coupled because, due to the orbital configuration, they have different symmetries with respect to the inversion around the middle points of nearest-neighbor bonds. So the ground-state degeneracy in this variational subspace is still equal to 3, supporting the interpretation in terms of chains.

When the ground state is at the K point, the interpretation is not so straightforward. The ground state is strictly speaking twofold degenerate. But looking at the spectra the first excited state is at the Γ point and very close to the ground state. A possible explanation could be that all these states are degenerate in the thermodynamic limit. Then this region could also be explained by the formation of chains. To check this point, we have diagonalized the Hamiltonian in the variational sub-space spanned by the three mean-field ground state wave functions of Phase D. The orbital configuration is different from Phase B, and the degeneracy is partially lifted, with a twofold degenerate ground-state an a nondegenerate excited state. Again the agreement supports the interpretation of this phase in terms of AF chains.

The most interesting region for our case is the central one. We will focus our attention on the line $t'/t=0$. Along this line we will see that a description in terms of resonating valence bond (RVB) states is reasonable. For instance, the low-lying spectrum (Fig. 14) for $J/U=0.008$ and $t'/t=0$, shows a very large number of singlet states (125) before the first triplet (at the top of the figure). All these singlets are very close in energy, the energy difference between the ground state and the first triplet being of the order of $\sim t^2/U$. Note that the number of singlets below the first triplet (125) is a significant fraction of the total number of dimer coverings for this 12-site cluster (348). This is reminiscent of the spectrum found by Lecheminant *et al.* for the $S=1/2$ Heisenberg model on the *kagome* lattice.[35]

This is in qualitative agreement with the mean-field results. Indeed, in Phases C and C', several solutions corresponding to various dimer coverings were found with comparable energies (see Figs. 15 and 16). A similar observation was made in a preliminary study of a similar spin-orbital model in the context of $BaVS_3$.[25]

Energy per site = −0.188077   Energy per site = −0.186959
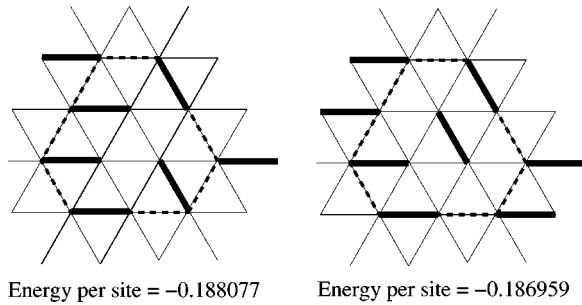
FIG. 15. Two stable states for a 12-site cluster: the dashed line represents the cluster. $t'/t=0$ and $J/U=0.008$.

A possible ground state for this region could be a spin-orbital version of the RVB state.[10] The magnetic structure could be envisaged as a fluctuating pattern of bonds among different dimer coverings or a mixture between dimer coverings and chains. All these states being singlets, they may be degenerate in the thermodynamic limit.

Let us also mention that there is also a partially polarized region $S=3$. We suspect that it may be a finite-size effect, as it is greatly reduced with respect to the corresponding $S=1$ phase present in the phase diagram of the tetrahedron.

VII. EXPERIMENTAL IMPLICATIONS

In transition metal oxides, the on-site Coulomb repulsion U is typically in the range 4–10 eV, and the Hund's rule coupling in the range 0.5–1 eV, leading to a physical range defined by $0.05 < J/U < 0.25$. Interestingly enough, all phases appear in this range and should be possible to observe in actual compounds provided the ratio t'/t has the appropriate value (see Fig. 16). In that respect, one should emphasize that the phase diagram depends only on the hopping integrals between orbitals, not on the actual orbitals. In particular, even if the two orbitals were not orthogonal by symmetry on one of the bonds, diagonalizing the hopping matrix on a given bond would bring us back to the situation treated in this paper. So the discussion would carry over beyond the specific case of $d_{3z^2-r^2}$ and $d_{x^2-y^2}$ up to the remarks dealing with Jahn-Teller distortions.

Now, coming back to LiNiO$_2$ and NaNiO$_2$, hence to $d_{3z^2-r^2}$ and $d_{x^2-y^2}$ orbitals, simple arguments suggest that t'/t *is negative and small*. That it is negative comes from the different symmetries of the orbitals: the $d_{3z^2-r^2}$ orbitals on

Energy per site = −0.187823   Energy per site = −0.188396
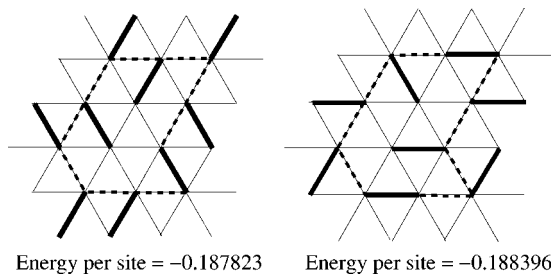
FIG. 16. Two stable states for another 12-site cluster: the dashed line represents the cluster. $t'/t=0$ and $J/U=0.008$.

edge-sharing octahedra (see Fig. 2) are symmetric with respect to the mirror plane that brings one octahedron into the other, while the $d_{x^2-y^2}$ are antisymmetric. Now any direct overlap between d wave functions in transition metal oxides is known to be very small. However, one should not forget that the orbitals are in fact Wannier functions centered on the transition metal ions, which extend in general to infinity to insure orthogonality, and which have a significant weight on neighboring O $2p$ orbitals. In the case of the Wannier orbitals with symmetry $d_{x^2-y^2}$, this does not lead to any significant transfer because the O $2p$ orbitals coupled to one of them are orthogonal to the $d_{x^2-y^2}$ of the neighboring octahedron. This is not strictly true here since the Ni-O-Ni angle is not exactly 90°, and also because the crystal field is not symmetric at the oxygen site, but still one expects the effective hopping to be very small. By contrast, the $d_{3z^2-r^2}$ Wannier orbitals have weight on the O $2p$ orbitals above and below, and these O $2p$ orbitals have a standard π overlap regardless of the actual local distortions of the octahedra. So this should give rise to a significant overlap between the Wannier functions with $d_{3z^2-r^2}$ symmetry.

Beyond the actual value of the parameters, it is important to emphasize that we have not adopted the same point of view as Mostovoy and Khomskii,[1] who have neglected any overlap between Ni orbitals, although it is allowed by symmetry. Further, they have assumed that Ni–O–Ni bonds make and angle of 90°, although the actual angle is around 94° in LiNiO$_2$ and 96.4° in NaNiO$_2$, and they have neglected the role of the crystal field at the oxygen site, known to produce antiferromagnetic couplings as shown by Daré, Hayn, and Richard.[21] While the ferromagnetic coupling that comes out of these approximations is certainly relevant, the simplified Hamiltonian studied by Mostovoy and Khomskii leads to a purely ferromagnetic coupling, while the more general Hamiltonian studied in the present work exhibits a rich variety of phases, which, we believe, might actually lead to the ultimate explanation of LiNiO$_2$ and NaNiO$_2$.

A. LiNiO$_2$

In the case of LiNiO$_2$, which undergoes neither a Jahn-Teller distortion nor a magnetic phase transition upon lowering the temperature, we have to choose between two different realizations of RVB: the SU(4) phase A (for $t \approx t'$) and the fluctuating dimer phases C and C'. Since we have argued that $|t'/t| \ll 1$, we opt for the dimer phases. Actually, one should give preference to Phase C' since t'/t is negative, but as we discussed these phases should better be considered as defining a domain in which the physics of the quantum dimer model (QDM) on the triangular lattice might be relevant. The actual form of the effective QDM is not known yet, but it presumably will not be too far from the minimal model studied by Moessner and Sondhi[36] since Phase C is a staggered state and belongs to the ground-state manifold of their model for large enough repulsion between face-to-face dimers, while Phase C' is a maximally flippable state and belongs to the ground state manifold in the limit of infinite attraction between face-to-face dimers. Note, however, that Phase C' is *not* the columnar state realized for finite attraction in the

minimal model, differences are to be expected. Still, close to the boundaries between the phases, one may speculate that an RVB phase will be present. Such a phase does not break any symmetry and could explain the absence of any kind of ordering in LiNiO$_2$. Let us also note that the extended x-ray-absorption fine-structure results by Rougier, Delmas, and Chadwick[6] are also consistent with this proposal since the orbitals entering all these states are Jahn-Teller orbitals with two long bonds and four short bonds. If the system undergoes resonances between different states, this would produce a dynamic Jahn-Teller effect between these states, a situation still leading to two long bonds and four short bonds on average. Due to some disorder, and/or to coupling to the lattice, the system might actually prefer to freeze in a nonperiodic dimer covering of the triangular lattice, as suggested by Reynaud et al.[12] Such a frozen, nonperiodic state would also be consistent with the results of Ref. 6.

B. NaNiO$_2$

As far as NaNiO$_2$ is concerned, the only potential candidate is Phase D since this is the only ferro-orbital phase with Jahn-Teller orbitals consistent with the distortion that occurs at 480 K in that system. This phase has the largest boundary with Phase C', a good point in view of the very similar structures of LiNiO$_2$ and NaNiO$_2$. As stated earlier, the effective model consists of weakly coupled AF chains, and the resulting magnetic structure will depend on the residual couplings. A thorough analysis of this point will require going beyond the present calculation and is left for future investigation. But in any case, with some interlayer coupling, this is expected to lead to some kind of AF ordering at finite temperature, in agreement with experiments. Let us emphasize that, while simultaneous ferromagnetism *and* Jahn-Teller active ferro-orbital order have been argued to be possible by Mostovoy and Khomskii[1] in the context of their simplified model, this seems to be impossible in the context of our microscopic model. Now, as far as experiments are concerned, the actual order is not yet known. It has been often assumed so far that this AF state consists of ferromagnetic planes coupled antiferromagnetically, but preliminary results seem to indicate that this cannot be the case,[37] which opens the way for another type of antiferromagnet.

C. Curie-Weiss constant

In the absence of finite-temperature calculations, we identify the Curie-Weiss constant θ_{CW} as a measure of the average spin couplings ($\propto \langle h_{ij}^T \rangle$). At this stage, the essential problem when comparing our predictions to the experimental data for LiNiO$_2$ and NaNiO$_2$[5] is the sign of the Curie-Weiss constant. Namely, in both cases it is ferromagnetic if determined at not too high a temperature,[12] while in our calculation, based on Eq. (22), it is antiferromagnetic. This is not a very serious problem, however. In deriving our model, we have only kept second-order terms in the hopping t and t' between Wannier orbitals centered at Ni sites. This derivation neglects intersite Coulomb processes. For symmetry reasons, the interaction is still of the form of Eq. (17); one of the terms would be the ferromagnetic direct exchange. We do
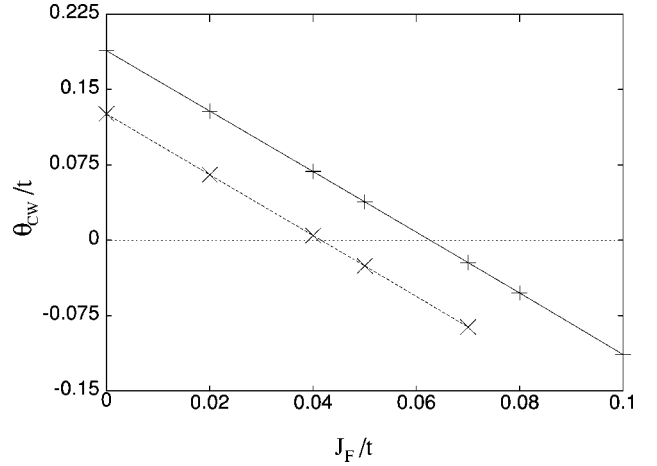
FIG. 17. θ_{CW} as a function of J_F for C and D phases (see Fig. 8): $J/U = 0.064$ and $t'/t = -0.1$ for the solid line (D phase), $t'/t = 0.1$ for the dashed line (C phase).

not handle this systematically, but include an *ad hoc* ferromagnetic term

$$H = -J_F \sum_{i,j} \mathbf{S}_i \cdot \mathbf{S}_j \qquad (40)$$

into the Hamiltonian ($J_F > 0$), which corresponds to modifying the initially antiferromagnetic B' term in Eq. (17) toward ferromagnetic couplings. We have checked that the phases discussed in Sec. V remain stable in a region where the Curie-Weiss constant is ferromagnetic. More precisely, we have solved the self-consistent equations including such a term, which leads to the effective spin Hamiltonian

$$H = \sum_{i,j} \{ (\mathbf{S}_i \cdot \mathbf{S}_j) h'_{ij} + k_{ij}^T \} \qquad (41)$$

where $h'_{ij} = \langle h_{ij}^T \rangle - J_F$, and the Curie-Weiss constant is given by

$$\theta_{CW} = \frac{S(S+1)}{3} \sum_{j(i)} h'_{ij} = \frac{1}{2} \sum_{\langle ij \rangle} {}' h'_{ij} \qquad (42)$$

where $\sum_{j(i)}$ means summation over all first neighbors of a given site i, while $\sum'_{\langle ij \rangle}$ means summing over three pairs of nearest-neighbors in three inequivalent directions. The results are summarized in Fig. 17. As announced, the Curie-Weiss temperature changes sign inside Phases C and D before one enters the ferromagnetic phase, and this occurs for values of J_F that are small enough to be physically relevant.

D. Comparison with previous approaches

We have emphasized on a number of occasions the difference between our model and the models studied in former investigations of these systems, in particular by Mostovoy and Khomskii[1] and by Daré, Hayn, and Richard.[21] For the sake of clarity, let us summarize these differences.

First of all, let us emphasize that the model of Eq. (17) is completely general, and that all models [those of Refs. 1 and 21 as well our Eq. (22)] are particular cases of this model.

The difference lies in the choice of the parameters, which are derived from different microscopic assumptions.

One formal difference between our approach and both that of Mostovoy-Khomskii and of Daré, Hayn, and Richard is that we consider Ni-like orbitals only. This does not mean that we neglect the presence of oxygen atoms, rather one should envisage d-p hybridization giving rise to an effective d-electron model.

The main difference between our approach and former approaches is the inclusion in our model of a significant direct hopping t between Ni Wannier functions for $d_{3z^2-r^2}$ orbitals on neighboring octahedra that share an edge perpendicular to the z axis, an effective hopping taking place through apical oxygens. This process is the main source of antiferromagnetic coupling in our approach. This should be contrasted with the model of Mostovoy and Khomskii in which all in-plane couplings are ferromagnetic, and with the model of Daré, Hayn, and Richard in which antiferromagnetic couplings arise from crystal field splittings and deviations of the (Ni–O–Ni) bond from 90°. This antiferromagnetic coupling competes with the other sources of exchange, which are ferromagnetic, as emphasized in previous work.[1,21] This competition is at the root of the very rich phase diagram we have obtained. In the derivation of their model, Mostovoy and Khomskii include an intersite Coulomb term, which we did not consider; on the other hand, we include hoppings, which they set to zero. Our phase diagram is therefore different in essential aspects from that of Mostovoy-Khomskii. It is a matter of further investigation, which of the parameter choices is more realistic, or whether suitably general models could give new phases.

The choice to emphasize this process has other technical implications, however, which translate into completely different expressions for the parameters of the Hamiltonian of Eq. (17). The reason is that, in terms of atomic orbitals, this process would be a rather high-order process, although simple estimates suggest that this overlap is significant. So the only practical way to include it into a microscopic model is to describe the system in terms of Wannier functions centered at the Ni sites rather than using atomic orbitals at Ni *and* O sites. So our effective Ni–Ni hopping parameters are not simply related to the atomic parameters of Refs. 1 and 21, and a direct comparison is not possible.

Still the basic assumptions of Mostovoy and Khomskii[1] and of Daré, Hayn, and Richard[21] regarding the other exchange processe are present in our model, but in a somewhat different disguise: (a) The fact that the Ni–O–Ni bond is nearly 90° is encoded in the fact that t', the effective hopping between d_{x2-y2} orbitals, is very small. (b) Deviations from this geometry, as well as the effect of crystal field splittings at the oxygen site, which were shown to lead to some AF exchange, translate into a non zero value of t'. (c) The ferromagnetic coupling that takes place at the non-apical oxygen sites was introduced phenomenologically as an extra ferromagnetic contribution in the previous section. A more direct comparison of the models should be possible starting from atomic orbitals and including a direct hopping between apical oxygen atoms. This is left, however, for future investigation.

VIII. CONCLUSION

We have shown that a spin-orbital model on the triangular lattice with realistic parameters leads to a very rich physics. The presence of various important phases [SU(4), dimers and ferromagnetic] is confirmed for every cluster (4, 12, and 16 sites). Moreover it seems that this model is able to provide a good description of the behavior of LiNiO$_2$ and NaNiO$_2$, and to explain the puzzling difference between these two compounds. We have given specific meaning to the claim that an RVB state seems to be at the origin of the magnetic properties of LiNiO$_2$. The underlying orbital structure corresponding to this RVB state is in agreement with the experimental observations. For the case of NaNiO$_2$, a possible magnetic state has been investigated with an underlying orbital structure that still leads to a cooperative Jahn-Teller distortion. A precise description of the low-energy physics of the present model for the phases relevant for LiNiO$_2$ and NaNiO$_2$ requires other methods than those used in the present paper, but we are confident that the present analysis will set the stage for further investigations.

[1] M. V. Mostovoy and D. I. Khomskii, Phys. Rev. Lett. **89**, 227203 (2002).

[2] E. Chappel, M. D. Nunez-Regueiro, G. Chouteau, O. Isnard, and C. Darie, Eur. Phys. J. B **17**, 615 (2000).

[3] K. Yamaura, M. Takano, A. Hirano, and R. Kanno, J. Solid State Chem. **127**, 109 (1996).

[4] Specifically, we mean the E derived from e_g. It will mix with the E derived from t_{2g}, but this effect does not appear explicitly in our reasoning.

[5] E. Chappel, M. D. Nunez-Regueiro, F. Dupont, G. Chouteau, C.

Darie, and A. Sulpice, Eur. Phys. J. B **17**, 609 (2000).

[6] At least not to an identifiable long-range pattern. EXAFS studies [A. Rougier, C. Delmas, and A. V. Chadwick, Solid State Commun. **94**, 123 (1995)] indicate that there is a local distortion at every Ni site, but the distortion pattern is frustrated, and does not support an (orbital) ordering transition

[7] K. Hirota, Y. Nakazawa, and M. Ishikawa, J. Phys.: Condens. Matter **3**, 4721 (1991).

[8] Y. Kitaoka, T. Kobayashi, A. Koda, H. Wakabayashi, Y. Niino, H. Yamakage, S. Taguchi, K. Amaya, K. Yamaura, M. Takano, A.

Hirano, and R. Kanno, J. Photogr. Sci. **67**, 3703 (1998).

[9] For a review, cf. A. M. Oleś, M. Cuoco, and N. B. Perkins, in *Lectures on the Physics of Highly Correlated Electron Systems*, edited by F. Mancini, AIP Conf. Proc. 527 (New York, 2000), p. 226.

[10] P. W. Anderson: Mater. Res. Bull. **8**, 153 (1973).

[11] P. Fazekas and P. W. Anderson, Philos. Mag. **30**, 423 (1974); B. Kleine, E. Müller-Hartmann, K. Frahm, and P. Fazekas, J. Phys.: Condens. Matter **87**, 103 (1992).

[12] F. Reynaud, D. Mertz, F. Celestini, J.-M. Debierre, A. M. Ghorayeb, P. Simon, A. Stepanov, J. Voiron, and C. Delmas, Phys. Rev. Lett. **86**, 3638 (2001).

[13] K. Hirakawa, H. Kadowaki, and K. Ubukoshi, J. Phys. Soc. Jpn. **54**, 3526 (1985).

[14] T. Arimori and S. Miyashita, J. Phys. Soc. Jpn. **69**, 2250 (2000).

[15] K. Penc, M. Mambrini, P. Fazekas, and F. Mila, Phys. Rev. B **68**, 012408 (2003).

[16] K. I. Kugel and D. I. Khomskii, Sov. Phys. Usp. **25**, 232, (1982).

[17] C. Castellani, C. R. Natoli, and J. Ranninger, Phys. Rev. B **18**, 4945 (1978).

[18] Spin-orbital states should be classified according to the double group belongig to $\mathcal{D}_{3d}$. This would be important if we included the effect of the relativistic spin-orbit interaction. In the present work, we assume that the spin and orbital Hilbert spaces are decoupled, and total spin eigenstates can be combined with point group basis states.

[19] We could have chosen the inversion instead of σ_h.

[20] For pairs of different orientation, or situated elsewhere in the lattice, $\mathcal{C}_2$ or/and σ_h should have been chosen differently. Summing over all pairs, the resulting Hamiltonian respects the space group symmetry of the lattice.

[21] A. M. Daré, R. Hayn, and J. L. Richard, Europhys. Lett. **61**, 803 (2003).

[22] Apart from a remark that the effect of J_H is insignificant. Our phase diagrams (Figs. 8 and 13) show that new phases are found at $J_H \neq 0$.

[23] Y. Q. Li, M. Ma, D. N. Shi, and F. C. Zhang, Phys. Rev. Lett. **81**, 3527 (1998).

[24] This choice of order parameters is permissible in the absence of spin–orbit coupling. With the spin–orbit coupling included, the right choice would be to use operators which are basis elements for the irreps of the $\mathcal{D}_{3d}$ double group.

[25] G. Mihály, I. Kézsmárki, F. Zámborszky, M. Miljak, K. Penc, P. Fazekas, H. Berger, and L. Forró, Phys. Rev. B **61**, R7831 (2000).

[26] In the sense that the fluctuating antiparallel correlations of a singlet are extrapolated to the antiparallel correlations of quasiclassical antiferromagnetic order. For spin–orbital models, the reasoning cannot be so straightforward.

[27] We note that the cubic e_g doublet system has a Hartree–Fock instability against T^y-polarization at non-integral fillings, though this solution does not seem motivated by the spin–orbital Hamiltonian [A. Takahashi and H. Shiba, J. Phys. Soc. Jpn. **69**, 3328 (2000)].

[28] For a pair of different orientation, it would be axial symmetry about a different direction in pseudospin space. It is for this reason that axial symmetry of the pair cannot be restated as a global symmetry of the lattice.

[29] Note that this section of the line is not a phase boundary, but it lies inside the ($S=1$, $T=0$) phase. Selecting the nondegenerate state $|ab\rangle - |ba\rangle$ does not require any special orbital symmetry.

[30] F. Mila, Phys. Rev. Lett. **81**, 2356 (1998).

[31] We are not too worried about this point for the following reason: the tetrahedral symmetry is atypically high, and probably gives a too large preference to SU(4) solutions. $N > 4$ pieces of the triangular lattice (even with periodic boundary conditions imposed) are less symmetrical.

[32] This was clearly established for the 1D case, where the energy is dominated by the mean-value of the four operator term. See e.g., B. Frischmuth, F. Mila, M. Troyer, Phys. Rev. Lett. **82**, 835 (1999).

[33] R. Coldea, D. A. Tennant, K. Habicht, P. Smeibidl, C. Wolters, and Z. Tylczynski, Phys. Rev. Lett. **88**, 137203 (2002) and references therein.

[34] B. Bernu, C. Lhuillier, and L. Pierre, Phys. Rev. Lett. **69**, 2590 (1992).

[35] P. Lecheminant, B. Bernu, C. Lhuillier, L. Pierre, and P. Sindzingre, Phys. Rev. B **56**, 2521 (1997).

[36] R. Moessner and S. L. Sondhi, Phys. Rev. Lett. **86**, 1881 (2001).

[37] G. Chouteau and S. de Brion (private communication); A. Jánossy (private communication).